

**DEVELOPMENT OF POLYMERIC HYDROGELS
AS BIO-GLUE**

THANAPON PUANGNIYOM

In Partial Fulfillment for the Degree of Bachelor of Science

Department of Chemistry, Faculty of Science

Chulalongkorn University

Academic Year 2020

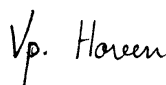
Project Title : Development of polymeric hydrogels as bio-glue
By : Thanapon Puangniyom ID. 6033034523
Field of study : Chemistry
Project Advisor : Associate Professor Dr.Voravee Hoven

Accepted by Department of Chemistry, Faculty of Science, Chulalongkorn University
in Partial Fulfillment of the Requirements for the Degree of Bachelor of Science

PROJECT COMMITTEE

1. Assistant Professor Dr.Varawut Tangpasuthadol Chairman
2. Assistant Professor Dr.Prompong Pienpinijtham Member
3. Associate Professor Dr.Voravee Hoven Project Advisor

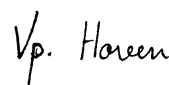
This report has been approved by Head of the Department of Chemistry



.....

(Associate Professor Dr.Voravee Hoven)

Project Advisor



.....

(Associate Professor Dr.Voravee Hoven)

Head of Department of Chemistry

Date 27 May 2021

| | |
|----------------------|--|
| ชื่อโครงการ | การพัฒนาพอลิเมอร์ไฮโดรเจลเป็นกาวชีวภาพ |
| ชื่อนิติในโครงการ | นายชนพล ปวงนิยม เลขประจำตัว 6033034523 |
| ชื่ออาจารย์ที่ปรึกษา | รองศาสตราจารย์ ดร.วรวิร์ โยเว่น |

บทคัดย่อ

การเย็บแผลด้วยไหมและลวดเย็บแผลมักใช้เพื่อปิดบาดแผลและส่งเสริมกระบวนการสมานแผลในร่างกาย อย่างไรก็ตามวิธีการที่กล่าวมานี้อาจทำให้เกิดความเสียหายเพิ่มเติมกับเนื้อเยื่อและไม่สามารถป้องกันการรั่วไหลของเหลวในร่างกายหรืออากาศได้ อีกทั้งไม่เหมาะสำหรับขั้นตอนการผ่าตัดเล็กในบริเวณที่มีการผ่าตัด จำกัด กาวติดเนื้อเยื่อหรือที่เรียกว่า "กาวชีวภาพ" กลายเป็นอีกทางเลือกหนึ่งที่น่าสนใจเนื่องจากช่วยให้การรักษาบาดแผลผ่านการยึดเกาะระหว่างเนื้อเยื่อและระหว่างเนื้อเยื่อกับพื้นผิวที่ไม่ใช่เนื้อเยื่อ ในงานวิจัยนี้ได้พัฒนาระบบพอลิเมอร์ไฮโดรเจลสองชนิดเพื่อใช้เป็นกาวชีวภาพ ชนิดแรกเป็นพอลิฟอสโฟเอสเทอร์สังเคราะห์ซึ่งเป็นหนึ่งในพอลิเมอร์ที่ย่อยสลายได้และเข้ากันได้กับร่างกายซึ่งสังเคราะห์จากมอนอเมอร์ 2 ตัว ได้แก่ 2-isopropoxy-1,3,2-dioxaphospholane-2-oxide (IPP) และ protected *N*-tyrosine-methyl-ester phospholane (P-TMP) ตามด้วยการกำจัดหมู่ปกป้อง โดยมีจุดประสงค์ให้โคพอลิเมอร์แบบสุ่มที่เกิดขึ้นของ poly(TMP-*r*-IPP) จะได้รับการเชื่อมขวางของหน่วยไทโรซีนในภาวะที่มี $[Ru(II)(bpy)_3]^{2+}$ และ โซเดียมเพอร์ซัลเฟต (SPS) หลังการฉายแสงขาว เพื่อสร้างเจลอ่อนที่สามารถใช้เป็นกาวชีวภาพ อย่างไรก็ตามผู้วิจัยไม่สามารถทำให้ P-TMP บริสุทธิ์ได้สำเร็จตามกำหนด จึงไม่สามารถศึกษาการสังเคราะห์โคพอลิเมอร์และการเกิดเจลได้ เพื่อบรรลุจุดประสงค์ข้างต้นได้ ชนิดที่สองเป็นพอลิแซ็กคาไรด์ที่ได้จากธรรมชาติ อัลจิเนตที่ดัดแปลงด้วยไทโรซีน (OAT) และควอเทอร์ไนซ์โคโตซาน (QC) ถูกเตรียมขึ้นผ่านการดัดแปลงทางเคมีของอัลจิเนตและโคโตซานตามลำดับ คาดว่า OAT และ QC จะสร้างไฮโดรเจลเครือข่ายแบบคู่ การเชื่อมขวางแบบปฏิกิริยาของพันธะอิมิน เกิดขึ้นระหว่างหมู่อัลดีไฮด์ใน OAT และหมู่อะมิโนใน QC ในขณะที่การเชื่อมขวางแบบทุติยภูมิเกิดขึ้น ผ่านเกิดเชื่อมขวางของหน่วยไทโรซีนของ AOT เมื่อได้รับการฉายแสงสีขาว การศึกษาเบื้องต้นชี้ให้เห็นว่า OAT ที่มีค่าการแทนที่ของไทโรซีน 16.8% มีแนวโน้มที่จะนำไปใช้ในการสร้างเจลต่อไปได้เนื่องจากสามารถละลายน้ำได้สูงถึง 2% w/v และเกิดเจลได้ภายใน 30 วินาที

คำสำคัญ: กาวติดเนื้อเยื่อ, พอลิฟอสโฟเอสเทอร์, การเชื่อมขวาง, การเชื่อมโยงฐาน Schiff, โคโตซาน, อัลจิเนต, แสงสีขาว, การเกิดเจล

Project Title : Development of the polymeric hydrogel as bio-glue

Student Name : Thanapon Puangniyom ID. 6033034523

Advisor : Associate Professor Dr.Voravee Hoven

Department of Chemistry, Faculty of Science, Chulalongkorn University, Academic Year 2020

ABSTRACT

Surgical sutures and staples are usually used to close wounds and improve wound healing process in our body. Nevertheless, they are still invasive and may cause additional damage to the tissues and cannot prevent body fluid or air leakage. They are not suitable for microsurgical procedures in a limited surgical site. Tissue adhesive or so-called “bio-glue” becomes an interesting alternative as it enables wound healing *via* the adhesion among tissues as well as between tissues to non-tissue surfaces. In this research, two polymeric hydrogel systems were developed to be used as bio-glue. The first system is based on a synthetic polyphosphoester, one of biodegradable and biocompatible polymer which was synthesized from two monomers namely, 2-isopropoxy-1,3,2-dioxaphospholane-2-oxide (IPP) and protected N-tyrosine-m-ester phospholane amidate (P-TMP) followed by deprotection. It was anticipated that the resulting random copolymer of poly(TMP-*r*-IPP) would undergo tyrosine crosslinking upon visible light irradiation in the presence of [RuII(bpy)₃]²⁺ and sodium persulfate (SPS) to form soft gel that can be applied as bio-glue. Unfortunately, we cannot successfully purify P-TMP in due course so that the investigation on the copolymerization and gelation cannot be fulfilled. The second system is based on naturally derived polysaccharides. Tyrosine-modified alginate (OAT) and quaternized chitosan (QC) were first prepared by chemical modification of alginate and chitosan, respectively. It was expected that OAT and QC would form a double network hydrogel. Primary crosslinking of imine bonds took place between aldehyde groups in the OAT and amino groups in the QC while the secondary crosslinking was formed *via* visible light-induced gelation of tyrosine units in the AOT. Preliminary investigation suggested that OAT with 16.8% substituted tyrosine seems to be a promising candidate to be further used for gel formation as it is water soluble with up to 2%w/v and it can form gel within 30 s.

Keywords: tissue adhesives, polyphosphoesters, crosslinking, Schiff base linkage, chitosan, alginate, visible light, gelation.

ACKNOWLEDGEMENT

First of all, I would like to express my sincere gratitude to my project advisor, Associate Professor Dr. Voravee Hoven, for giving me the opportunity to do my senior project including the financial support such as chemicals and laboratory instruments. Even though, the project is not completely done, I gain a lot of basic and advanced knowledge including laboratory experiences that they are important and necessary for future graduate study. Her guidance and support really helped educate and motivate me for facing research challenge in the future. I also owe my deepest gratitude to Professor Dr. Yasuhiko Iwasaki, for providing an original idea of this research project.

Special thank goes to Dr. Susita Noree. Not only is she my personal mentor who taught me a lot of fundamental knowledges and research skill required for my research, she is also very supportive and taking care of me well like her own brother. She always shares her opinion and give suggestions that are very valuable for my laboratory work and report. I really appreciate her kindness. Moreover, I also thank to other Hoven's research group members who are very helpful throughout my time in the laboratory. They always give me constructive comments and solutions for the problems that I cannot solve by myself. Especially, I would like to thank Tinnakorn Phuangkaew who assisted me in the synthesis of quaternized chitosan.

I have to thank Development and Promotion of Science and Technology Talents (DPST) scholarship for my undergraduate scholarship and Department of Chemistry, Faculty of Science for providing financial support for senior project. Moreover, I have to thank my best friends, ChemCU84 friends and my beloved family for their emotional support.

CONTENTS

| | PAGES |
|---|----------|
| ABSTRACT (TH) | iv |
| ABSTRACT (ENG) | v |
| ACKNOWLEDGMENTS | vi |
| CONTENTS | vii |
| LIST OF TABLES | x |
| LIST OF FIGURES | xi |
| LIST OF SCHEMES | xiv |
| LIST OF ABBREVIATIONS | xv |
| CHAPTER 1 | 1 |
| 1.1 INTRODUCTION | 1 |
| Part 1: Polyphosphoester-based hydrogel | 2 |
| Part 2: Polysaccharide-based hydrogel | 4 |
| 1.2 THEORY AND LITERATURE REVIEW | 8 |
| 1.2.1 The Mechanisms of Adhesion | 8 |
| 1.2.2 Coagulation process | 10 |
| 1.2.3 Antibacterial Activity | 11 |
| 1.2.4 Visible-photoinduced Crosslinking | 12 |
| 1.3 OBJECTIVES | 14 |
| Part 1: Polyphosphoester-based hydrogel | 14 |
| Part 2: Polysaccharide-based hydrogel | 14 |

CONTENTS

| | PAGES |
|--|-----------|
| CHAPTER 2 | 15 |
| EXPERIMENTAL METHOD | 15 |
| 2.1 Instrument | 15 |
| 2.2 Polyphosphoester-based hydrogel | 15 |
| 2.2.1 Materials | 16 |
| 2.2.2 Synthesis of 2-isopropoxy-1,3,2-dioxaphospholane 2-oxide (IPP) monomer | 16 |
| 2.2.3 Synthesis of methyl-3-(4-((tert-butyldimethylsilyl)oxy)phenyl)-2-(((2-oxido -1,3,2-dioxaphospholan-2-yl)oxy)amino)propanoate, protected N-tyrosine-m-ester phospholane amidate (P-TMP) monomer | 17 |
| 2.3 Polysaccharide-based hydrogel | 18 |
| 2.3.1 Materials | 18 |
| 2.3.2 Synthesis of tyrosine-modified alginate (AT) | 19 |
| 2.3.3 Gelation by visible light-induced crosslinking | 20 |
| 2.3.4 Synthesis of oxidized tyrosine-modified alginates (OAT) | 20 |
| 2.3.5 Determination of degree of tyrosine substitution on tyrosine-modified alginates | 20 |
| 2.3.6 Synthesis of quaternized chitosan (QC) | 21 |

CONTENTS

| | PAGES |
|--|-----------|
| CHAPTER 3 | 22 |
| RESULTS AND DISCUSSION | 22 |
| 3.1 Polyphosphoester-based hydrogel | 22 |
| 3.1.1 Synthesis of 2-isopropoxy-1,3,2-dioxaphospholane 2-oxide (IPP) monomer | 22 |
| 3.1.2 Synthesis of methyl-3-(4-((tert-butyldimethylsilyl)oxy)phenyl)-2-(((2-oxido -1,3,2-dioxaphospholan-2-yl)oxy)amino)propanoate, protected N-tyrosine-m-ester phospholane amidate (P-TMP) monomer | 22 |
| 3.2 Polysaccharide-based hydrogel | 30 |
| 3.2.1 Synthesis of oxidized tyrosine-modified alginate (OAT) | 30 |
| 3.2.2 Synthesis of quaternized chitosan (QC) | 36 |
| CHAPTER 4 | 39 |
| CONCLUSIONS | 39 |
| REFERENCES | 40 |
| VITA | 45 |

LIST OF TABLES

| | PAGES |
|---|-------|
| Table 3.1 AT products synthesized using different feeding of L-tyr mole equivalents and their solubilization in aqueous media at RT. | 36 |

LIST OF FIGURES

| | PAGES |
|---|-------|
| Figure 1.1 Examples of tissue injuries and primary functions of tissue adhesives. | 2 |
| Figure 1.2 Examples of synthetic polymers mimicking natural polymers. | 3 |
| Figure 1.3 Example molecules of COP derivatives | 4 |
| Figure 1.4 Overview of polyphosphoester-based hydrogel formation. | 4 |
| Figure 1.5 Structure of chitosan and chitosan derivatives related with their solubility. | 6 |
| Figure 1.6 Chemical modification of alginate backbone through oxidation using sodium periodate. | 7 |
| Figure 1.7 Overview of polysaccharide-based hydrogel formation and expected properties. | 8 |
| Figure 1.8 Schematic overview of tissue-adhesive interface. | 9 |
| Figure 1.9 Schematic of the coagulation process | 10 |
| Figure 1.10 Schematic representation of antimicrobial mechanisms of chitosan and its derivatives. | 12 |
| Figure 1.11 Toxicity of individual components to L929 mouse fibroblast cells <i>in vitro</i> . | 13 |
| Figure 1.12 Schematic representation of adhesion bonding between polysaccharide-based hydrogel and tissue surface. | 13 |
| Figure 3.1 ¹ H-NMR spectra of COP precursor and IPP monomer in CDCl ₃ | 22 |
| Figure 3.2 FT-IR spectra of L-tyrosine methyl ester, TBDMSCl and protected L-tyrosine methyl ester. | 23 |
| Figure 3.3 ¹ H-NMR spectra of L-tyrosine methyl ester in D ₂ O, TBDMSCl and protected L-tyrosine methyl ester in CDCl ₃ . | 24 |

LIST OF FIGURES

| | PAGES |
|---|-------|
| Figure 3.4 A) TLC results of standard PT, fraction, separated product in different mobile phase and B) ^{31}P -NMR spectra of crude product and separated product. | 25 |
| Figure 3.5 ^1H -NMR spectra of crude product and fraction 3, 4 in CDCl_3 . | 26 |
| Figure 3.6 A) ^1H -NMR and B) ^{31}P -NMR spectra of crude product of the first and second batches. | 27 |
| Figure 3.7 A) A setup of instrument used for silica gel plug method B) TLC spots of standard PT and crude product. | 28 |
| Figure 3.8 TLC spots of standard PT, crude product and fractions. | 29 |
| Figure 3.9 ^{31}P -NMR spectra of crude product and fraction 1, 2 and 3 and PA/PP ratio. | 29 |
| Figure 3.10 The possible products in the reaction and purification methods. | 30 |
| Figure 3.11 FT-IR spectra of A) sodium alginate, B) tyrosine-modified alginate and C) oxidized tyrosine-modified alginate. | 31 |
| Figure 3.12 Absorption spectra of sodium alginate compared with tyrosine-modified alginate. | 32 |
| Figure 3.13 Appearance of A) tyrosine-modified alginate (AT) and oxidized tyrosine-modified alginate (OAT) in aqueous media and B) 2,4-DNP test results to check aldehyde formation in AT and OAT. | 32 |
| Figure 3.14 Standard calibration curve of UV/Vis absorption as a function of tyrosine-m-ester concentration (0.01-1.0 mM). | 33 |
| Figure 3.15 Degree of tyrosine substitution (%DS) in AT versus reaction time. | 34 |
| Figure 3.16 Mechanism of a photo-initiated tyrosine crosslinking reaction. | 35 |
| Figure 3.17 Gelation of products <i>via</i> visible light-induced crosslinking by using ruthenium as catalyst. | 36 |

LIST OF FIGURES

| | PAGES |
|--|-------|
| Figure 3.18 FT-IR spectra of A) chitosan and B) quaternized chitosan. | 37 |
| Figure 3.19 ^1H -NMR spectra of A) chitosan and B) quaternized chitosan in CF_3COOH and D_2O . | 38 |

LIST OF SCHEMES

| | PAGES |
|---|-------|
| Scheme 2.1 Synthesis overview of polyphosphoester-based hydrogel. | 15 |
| Scheme 2.2 Synthesis of IPP monomer. | 16 |
| Scheme 2.3 Synthesis of protected L-tyrosine methyl ester. | 17 |
| Scheme 2.4 Synthesis of P-TMP monomer. | 17 |
| Scheme 2.5 Structures of quaternized chitosan and oxidized tyrosine-modified alginate to be used for hydrogelation <i>via</i> Schiff base linkage. | 18 |
| Scheme 2.6 Synthesis of oxidized tyrosine-modified alginate in 2 reaction steps. | 19 |
| Scheme 2.7 Synthesis of quaternized chitosan. | 21 |

LIST OF ABBREVIATIONS

| Abbreviation | Definition |
|---------------------|--|
| PPEs | Poly(phosphoester)s |
| ROP | Ring-opening polymerization |
| COP | 2-Chloro-1,3,2-dioxaphospholane-2-oxide |
| LCST | Lower critical solution temperature |
| COP | 2-Chloro-1,3,2-dioxaphospholane-2-oxide |
| IPP | 2-Isopropoxy-2-oxo-1,3,2-dioxaphospholane |
| P-TMP | Methyl-3-(4-((tert-butyldimethylsilyl)oxy)phenyl)-2-(((2-oxido-1,3,2-dioxaphospholan-2-yl)oxy)amino) or protected N-tyrosine-m-ester phospholane amidate |
| OAT | Oxidized alginate-tyrosine or oxidized tyrosine-modified alginate |
| QC | Quaternized chitosan |
| EDC | 1-Ethyl-3-(3-dimethylaminopropyl)carbodiimide |
| NHS | <i>N</i> -Hydroxysuccinimide |
| GTMAC | Glycidyltrimethylammonium chloride |
| L-tyr | <i>L</i> -Tyrosine-methyl-ester hydrochloride |
| IPA | 2-Propanol |
| TBDMSCl | <i>tert</i> -Butyldimethylsilyl chloride |
| SPS | Sodium persulfate |
| PA | Phospholane amidate |
| PP | Phosphate phospholane |
| DS | Degree of substitution |

CHAPTER 1

INTRODUCTION

1.1 Introduction

In each year, more than ten million people have suffered from a variety of tissue wounds ranging from minor skin cuts to severe injuries, such as traumatic incidents, chronic wounds such as diabetic ulcers, and surgical incisions. [1-3] Therefore, medical treatments for those injuries essentially enhance reconnection of the injured tissues and closure of the defect areas in order to stop bleeding, prevent leakage, and ultimately build up tissue structures and functions are certainly important issues. [4]

Traditionally, staples and sutures have been the first choice for wound treatment process. Both techniques can firmly approximate the tissues until they heal and resist mechanical loads such as stretching of tissues for reducing the risks of surgical wound dehiscence. [5,6] Even, these approaches have well improved wound and surgical care, they are often unsuitable in certain situations, for example, those that require leakage prevention of body fluids or air. Moreover, its challenge lies in achieving effective closure when wounds are large. On the other hand, they are not applicable to minimally invasive or microsurgical procedures in a limited surgical site. Therefore, new kinds of materials have been constantly researched and developed and one of promising biomaterials is tissue adhesives.

Tissue adhesives have been increasingly important elements in modern medicine, with rapid development over the past 30 years. The tissue adhesives enable the innate wound healing processes to occur through the adhesion of tissue to the tissue on-site or tissue to non-tissue surfaces on-site. An ideal tissue adhesive should possess a number of characteristics as shown in **Figure 1.1**, including 1) biological compatibility and nontoxicity, 2) suitable chemistry to create robust tissue adhesion, 3) mechanical similarity to the underlying tissue, 4) mechanical capacity to withstand repeated dynamic forces imposed by the tissue, 5) acceptable swelling profile to minimize tissue compression, and 6) biodegradability at a compatible rate related to tissue healing. [7-12] Recently, several classes of tissue adhesives have been developed, but there is still a serious concern due to toxicity and performance problems. For example, cyanoacrylate-based adhesives are brittle and release degradable formaldehyde products, [13] and the use of cyanoacrylate adhesives can cause inflammation and tissue necrosis. [14] Fibrin

sealants may exhibit poor adhesion and pose a risk of viral infection. [15-16] Thus, synthetic biomaterial sealants are alternatively sought to relieve these concerns.

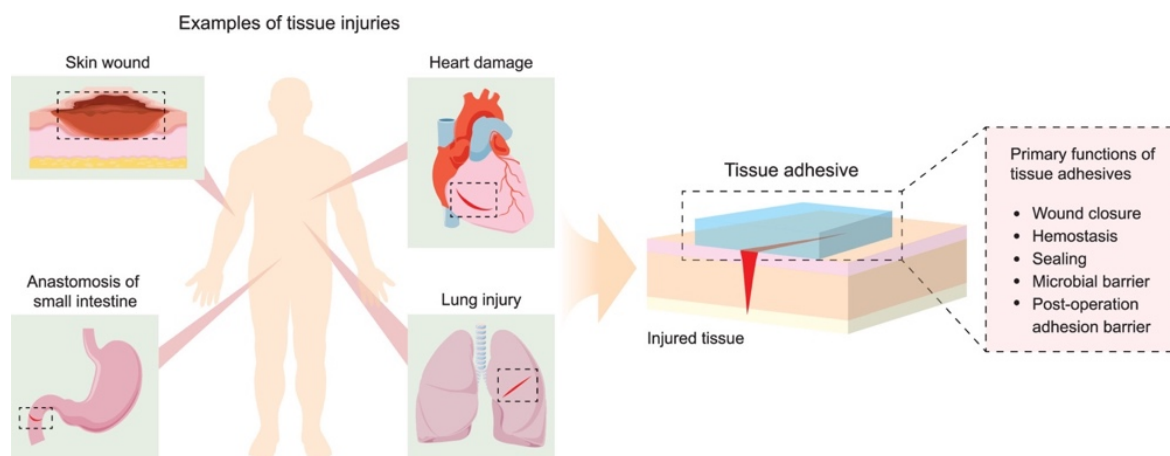


Figure 1.1 Examples of tissue injuries and primary functions of tissue adhesives. [2]

In this senior project studies, we have explored the possibility to develop tissue adhesives from two polymeric compounds, namely synthetic polyphosphoesters and naturally derived polysaccharide-based materials.

Part 1: Polyphosphoester-based hydrogel

Biopolymers have always inspired scientists to mimic their performance and properties as synthetic analogs (**Figure 1.2**). Elastomer as natural rubber derived from rubber trees and its deficiency in the past wars led to the development and the discovery of polyolefin chemistry. Polyesters are found in nature and have found increasingly used also as synthetic polymers. Polyamides provide polar amide bonds to share with natural proteins and an attempt is currently being undertaken to imitate the sequential control and the great mechanical properties offered by the polypeptide of spider web. [17]

In addition, synthetic main-chain poly(phosphoester)s (PPEs) are attractive candidates possessing biocompatibility and biodegradability because the similarity of their building blocks to natural nucleic acids, and their backbone is recognizable with enzymes and can be cleaved under physiological conditions. [18] Furthermore, hydrolytic degradation of the polyphosphoester backbone with or without an enzyme (*e.g.* phosphatase) also makes PPEs interesting for biomedical applications.

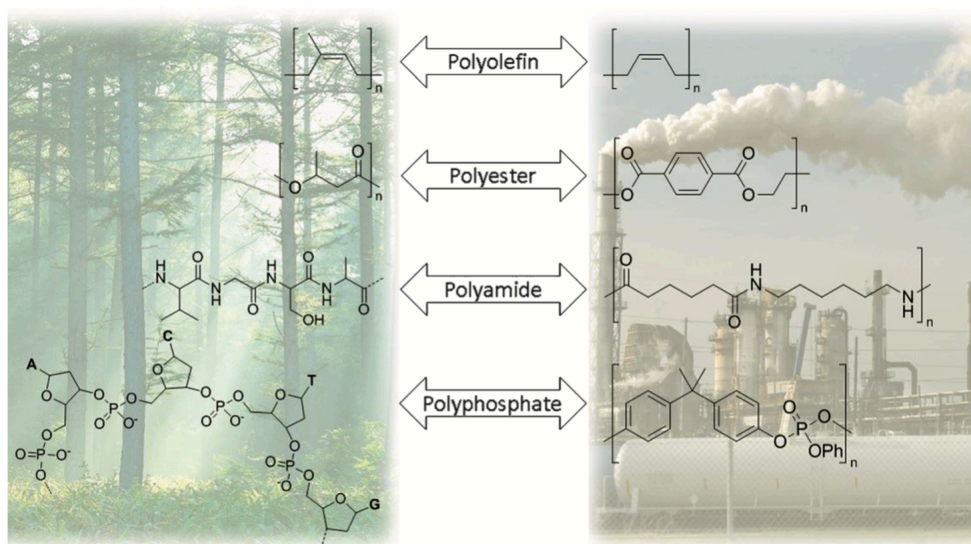


Figure 1.2 Examples of synthetic polymers mimicking natural polymers. [17]

Polyphosphoester as a class of biodegradable polymers has several advantages, including good biocompatibility, favorable biodegradability, facile functionalization. [19] Therefore, it can fully meet not only the requirements of the current drug delivery system but also tissue adhesives. Deoxyribonucleic acid/tannic acid (DNA/TA)-based hydrogel was performed by using intermolecular force as hydrogen bonding between catechol groups on tannic acid and bases on DNA structure. Phosphodiester bonds presented efficient tissue adhesiveness and can be an excellent hemostatic agent in coagulation process. [20]

PPEs were synthesized by ring-opening polymerization (ROP). 2-chloro-1,3,2-dioxaphospholane-2-oxide (COP), which is one of cyclic phospholane monomers, can be modified *via* nucleophilic substitution for replacing chlorine position to nucleophilic side chain groups (*O*-attack or *N*-attack) (**Figure 1.3**). The different functionalities of their side chain groups are easily tunable, endowing them with desirable mechanical, chemical, and biological potential, in contrast to other biodegradable polyesters (*e.g.*, polylactide and polycaprolactone). Examples of the phospholane monomer analogs with different functionalities are 2-(but-3-yn-1-yloxy)-2-oxo-1,3,2-dioxaphospholane (BYP), 2-ethoxy-1, 3, 2-dioxaphospholane (EEP), and 2-isopropoxy-2-oxo-1,3,2-dioxaphospholane (IPP). Iwasaki et al. reported the synthesis of a copolymer consisting of PEEP and PIPP which are thermo-responsive polymer by anionic ROP using triisobutylaluminum as an initiator. The copolymers with a composition of 24%

PIPP and 74% PEEP exhibit lower critical solution temperature (LCST) approximately 31°C *via* controlling the PIPP ratio in the polymer chain. [21]

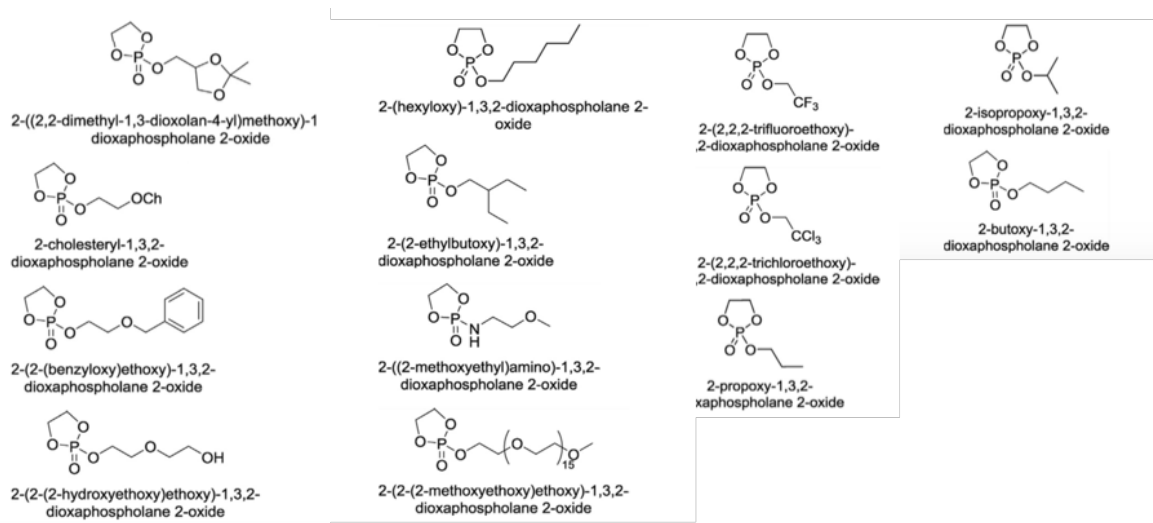


Figure 1.3 Example molecules of COP derivatives [62]

In this study, we would like to introduce thermo-responsive property to PIPP so it can be when applied on tissue surface by optimizing LCST of the synthesized copolymer. IPP monomer was copolymerized with methyl-3-(4-((tert-butyldimethylsilyl)oxy)phenyl)-2-(((2-oxido-1,3,2-dioxaphospholan-2-yl)oxy) amino) propanoate or protected *N*-tyrosine-*m*-ester phospholane amidate (P-TMP) monomer to prepare a copolymer of poly(TMP-*r*-IPP) which can form hydrogel upon visible light-induced crosslinking in the presence of ruthenium catalyst as shown in **Figure 1.4**. It is anticipated that this hydrogel can be used as biodegradable tissue adhesive or bio-glue.

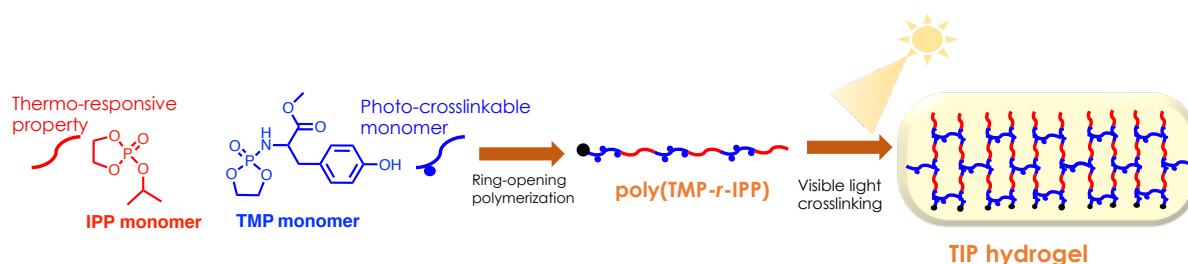


Figure 1.4 Overview of polyphosphoester-based hydrogel formation.

Part 2: Polysaccharide-based hydrogel

Dynamic covalent bonds, such as Schiff bases, disulfide bonds and Diels–Alder reactions have been employed for the preparation of hydrogels with various functions.

Especially, chitosan-based hydrogels constructed *via* Schiff bases have been widely explored as biomaterials for hemostasis, drug delivery, and bio-adhesives due to their good biocompatibility and biodegradability under physiological conditions. [22-23] For example, Liu and coworkers developed a chitosan/aldehyde-PEG to form self-healing hydrogel for use as bioink in 3D bioprinting and modular 3D bioprinting and the mechanical properties of hydrogel was enhanced by secondary crosslinking. [24] In bio-adhesive applications, antibacterial and anti-inflammatory properties of tissue adhesives play an important role in wound healing. [25] Synthetic materials had shown their excellent antibacterial and anti-inflammatory properties according to the previous reports. For example, functionalized poly(ethylene glycol)-*co*-poly(glycerol sebacate) was used to prepare antibacterial, antioxidant, and electroactive dressing for cutaneous wound healing. [26] However, some synthetic materials have those properties, but they cannot degrade in physical environment. It was a sensible choice to select natural polymers as the tissue adhesives *via* chemical modifications.

Chitosan is a linear natural polysaccharide, partially deacetylated derivative from chitin. Chitosan has been widely used in drug delivery and tissue engineering because of its excellent biocompatibility, biodegradability, hemostatic properties and antibacterial properties [27]. For its strong inter-molecular hydrogen bonding, chitosan has poor solubility in physiological solvents, which limited its applications in tissue engineering. [28] To get rid of this disadvantage, polymeric quaternary ammonium compounds have received the most attention over the years to improve solubility of chitosan in physical condition as exhibited in **Figure 1.5** and still have antimicrobial properties. Liu and coworkers reported quaternized chitosan exhibiting antimicrobial properties against microorganisms such as *Escherichia coli*, *Staphylococcus aureus* [29] and it has been rarely investigated in tissue adhesive fields.

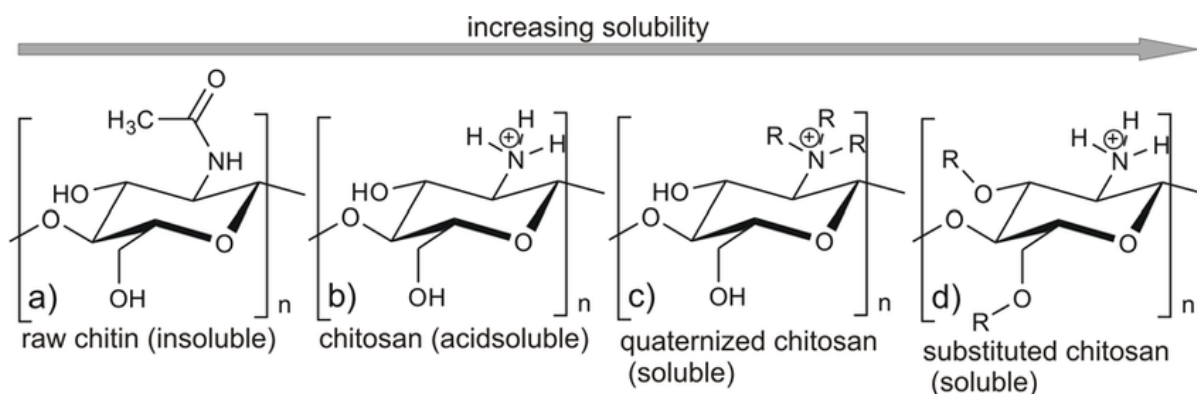


Figure 1.5 Structure of chitosan and chitosan derivatives related with their solubility. [30]

Alginate is a linear and naturally occurring anionic and hydrophilic polysaccharide containing blocks of (1–4)-linked β -D-mannuronic acid (M) and α -L-guluronic acid (G) monomers [31]. Alginate has been extensively investigated and used for many biomedical applications due to its biocompatibility, biodegradability and relatively low cost, as well as excellent gel-forming properties by addition of divalent cations such as Ca^{2+} [32] and was easily modified *via* carboxylate groups on each unit. Unfortunately, Alginate is biologically inert and inherently nondegradable in the body due to the lack of enzymes that can cleave the polymer chains and low tissue adhesiveness. Therefore, alginate is often oxidized into dialdehyde for use in the body, creating hydrolytically labile bonds as shown in **Figure 1.6**. [33] Moreover, the aldehyde groups on alginate can react with amino groups on modified chitosan and primary amine on amino acid *via* the Schiff-base linkage [34]. In previous paper, Yuan and coworkers presented that aldehyde of oxidized alginate was crosslinked with gelatin to form soft tissue adhesive. [35] The results found that its adhesive strength equal to the commercial adhesive fibrin glue and the ratio of the alginate to gelatin could be tunable. Thus, these hydrogels could be a promising candidate as tissue adhesive for bio-applications

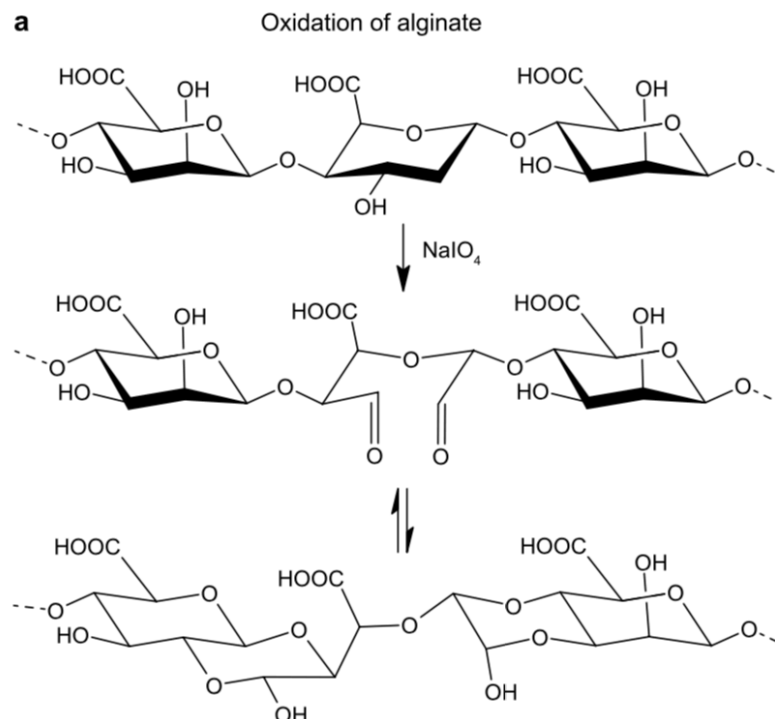


Figure 1.6 Chemical modification of alginate backbone through oxidation using sodium periodate. [2]

In this study, we aimed to develop polysaccharide-based hydrogel *via* Schiff-base linkage between oxidized alginate-tyrosine (OAT) and quaternized chitosan (QC) to generate as bio-glue as tissue adhesive. Moreover, visible light-induced crosslinking was induced after Schiff-base formation to reinforce the gel. We hypothesized that this double network hydrogel would exhibit good characteristics that are suitable to be used as tissue adhesive as shown **Figure 1.7**. It should also be clinically applicable such as being less traumatic closure and suffering, easy application, no stitches required after surgery, excellent cosmetic result, and localized drug release.

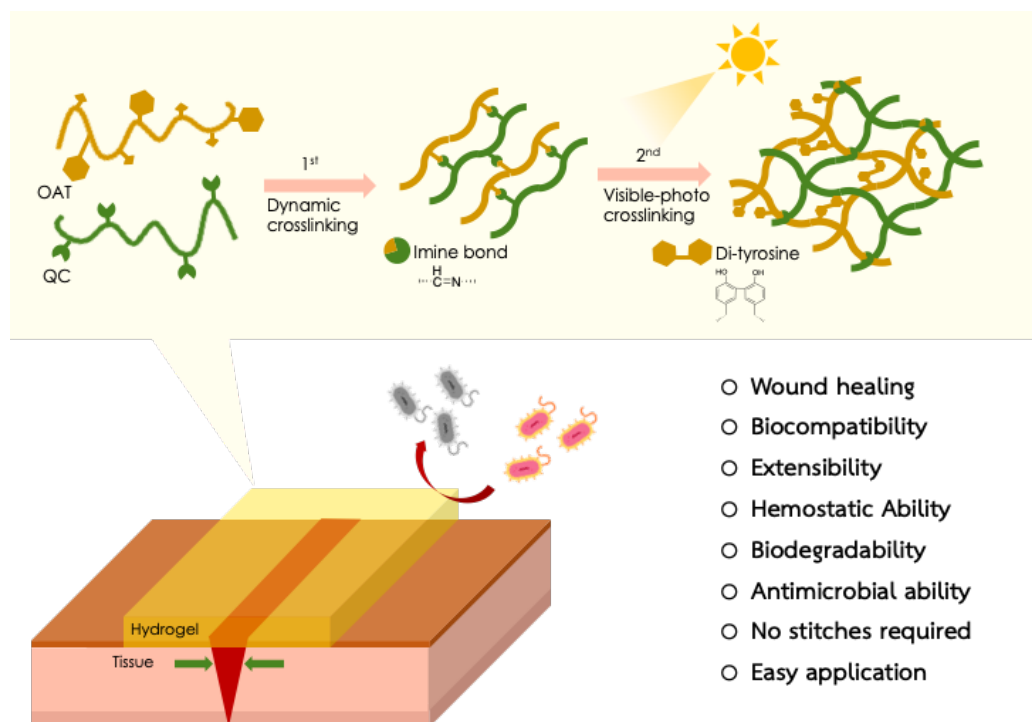


Figure 1.7 Overview of polysaccharide-based hydrogel formation and expected properties.

1.2 Theory and Literature Review

1.2.1 The Mechanisms of Adhesion

The key function of a tissue adhesive is to form strong adhesion between tissues and adhesives surface under physiological conditions, which can limit adhesiveness of the adhesives among the wet environment due to blood and body fluids. [36] The main adhesion mechanisms of these tissue adhesives include molecular bonding, mechanical coupling, and thermodynamic adhesion [37]. Among them, molecular bonding is the most popular explanation. Briefly, interatomic and intermolecular forces occur between the molecules on the tissue and adhesive surface, involving hydrogen bonding, capillary forces, Van der Waals forces, static electric forces, and covalent bonds as shown in **Figure 1.8**.

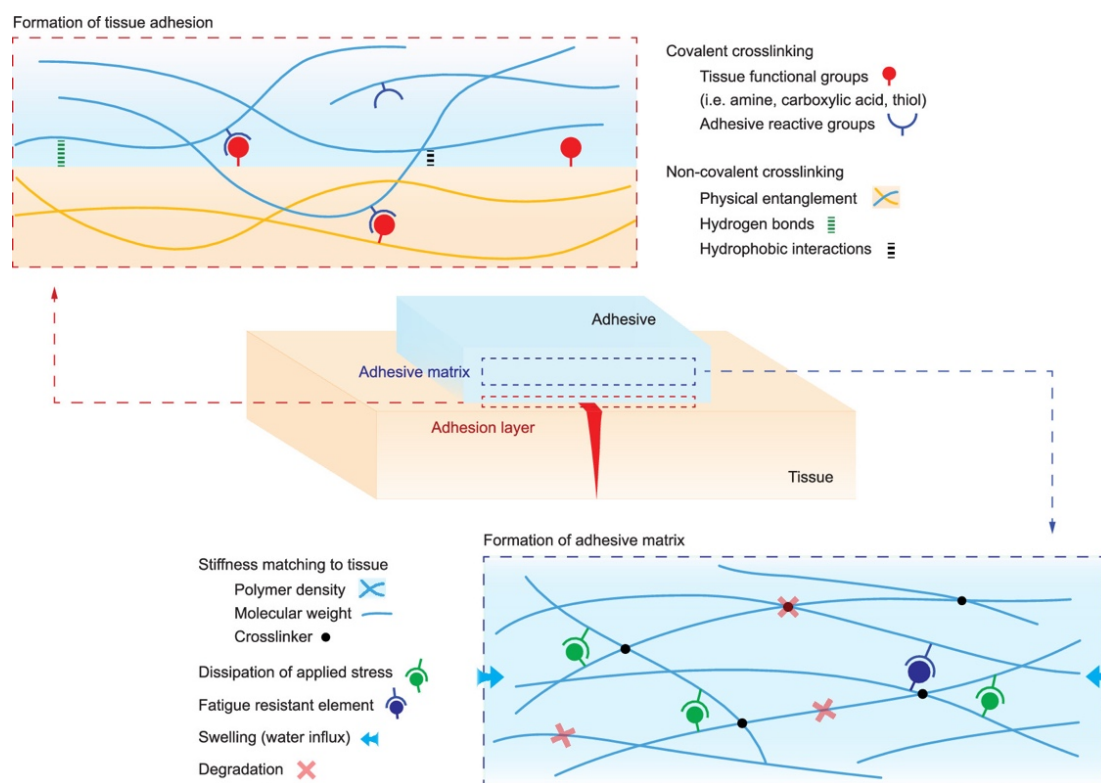


Figure 1.8 Schematic overview of tissue-adhesive interface. The interface can be spatially divided into two regimes; adhesion layer and adhesive matrix. The adhesion layer forms tissue adhesion through covalent and noncovalent cross-linking mechanisms (upper box). The adhesive matrix largely determines the physicochemical properties of the adhesive (lower box). [2]

Chemical functional groups presented on the tissue surface allow for covalent interactions with adhesives, and functional groups originating from amino acid residues in proteins which are particularly prominent targets. Whereas basic amino acids with positively charged residues such as lysine provide primary amines (*i.e.*, ϵ -amines), acidic amino acids such as glutamic acid contribute carboxylic acids. [38] Additional primary amines (*i.e.*, α -amines) and carboxylic acids at the C- and N-ends of a polypeptide, imidazole from histidine, and thiol from cysteine also contribute to the available tissue functional groups. [39] They are able to initiate a variety of chemical reactions by providing an active electron pair for conjugation with the reactive groups of tissue adhesives for forming covalent bonding between tissue surface and hydrogel surface.

1.2.2 Coagulation process

Coagulation is a complicated process of plasma transformation from an unstable platelet plug to stable and insoluble fibrin, which is a body's multifaceted response to bleeding. This process is divided into two hemostasis steps as displayed in **Figure 1.9**. Initial platelet plug is formed in the primary hemostasis when the vascular wall is injured. Inactive platelets circulating in blood become activated, subsequently. Platelets trigger an aggregation of other locally activated platelets. Fibrin in the secondary hemostasis is then formed, when the coagulation cascade is initiated. The clotting factor involved in this stage is activated gradually. Activated X cleaves prothrombin into thrombin, then fibrinogen is cleaved into fibrin monomers by the enzymolysis of thrombin. Finally, the fibrin monomers are crosslinked with Ca^{2+} and subsequently activated factor XIII to stable fibrin clot on tissue injuries. [40]

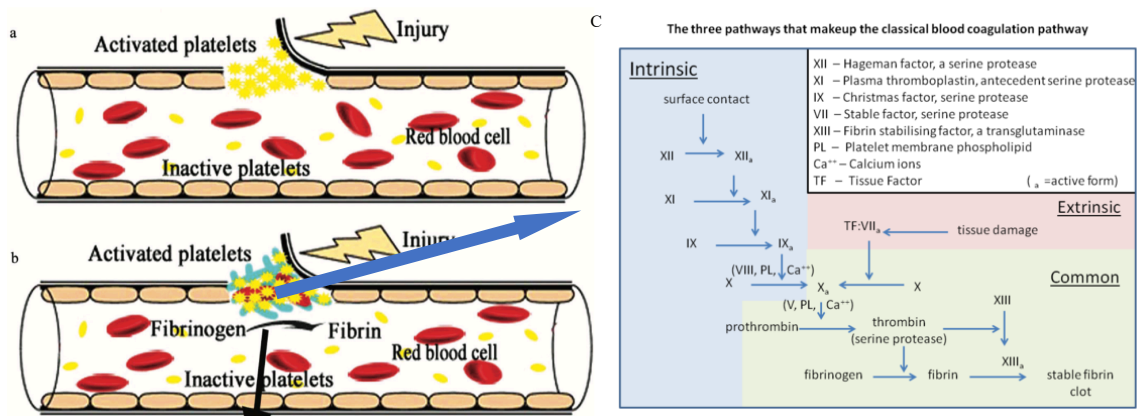


Figure 1.9 Schematic of the coagulation process: (a) the primary hemostasis (b) the secondary hemostasis (c) Process of the coagulation cascade, which includes intrinsic and extrinsic coagulation pathways (including the common pathway). [41-42]

In case of polyphosphoester-based materials, the polymer chain contains plenty of electively charges due to phosphoester moieties that can induce positive factors in coagulation process *via* active pathway. On the other hand, polysaccharide-based materials, hemostatic mechanisms can be divided into the active pathway and the passive pathway.

1. The active pathway includes directly activating the coagulation cascade to begin the coagulation process or contribute to the coagulation process. Besides, for the polysaccharide-based materials, hemostatic dressings based on chitosan and alginate are

capable of facilitating fibrin clot formation. For instance, the positively charged surface on the chitosan can adhere platelets *via* charge interaction and the negatively charged surface of alginate can induce coagulation initiating *via* the autoactivation of coagulation factor XII. [43]

2. The passive pathway needs to possess surface properties of materials. The modification of material surface was found to improve the hemocompatibility. [44] It is reported that surface modification of PEG, zwitterionic polymers, heparin and bioactive macromolecules (such as gelatin, and serum albumin) can improve anti-platelet adhesion and anti-protein adsorption abilities. For example, polysaccharide-based materials, such as oxidized regenerated cellulose (ORC) gauze and starch-based microspheres, can instantly extract fluid from blood when applying to an active bleeding site, causing proteins, platelets, red blood cells and other effective components of blood concentrate on the material surface. [45]

1.2.3 Antibacterial Activity

The exact mechanism of antibacterial activity is yet clearly understood. The most prevalent proposed antibacterial activity of chitosan is by binding to the negatively charged bacterial cell wall causing disruption of the cell, thus altering the membrane permeability, followed by attachment to DNA causing inhibition of DNA replication and subsequently cell death as **Figure 1.10**. [46]. Another possible mechanism is that chitosan acts as a chelating agent that electively binds to trace metal elements causing toxin production and inhibiting microbial growth [47].

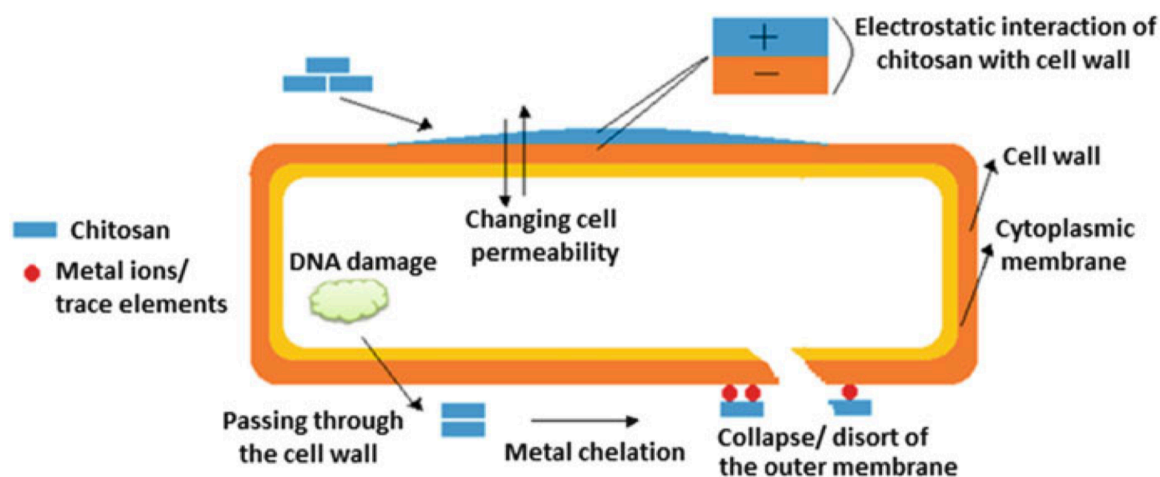


Figure 1.10 Schematic representation of antimicrobial mechanisms of chitosan and its derivatives. [48]

For the quaternized chitosan, Liu and colleagues had been reported that modifying chitosan *via* quaternization can improve antimicrobial property of its materials according to quaternization degree. [29]

1.2.4 Visible light-induced Crosslinking

There are various methods for improving mechanical properties of hydrogel. The most well-known approach is secondary photo-crosslinking by using ultraviolet (UV) or visible light. For example, methacrylated chitosan was formed into 3D constructs and stabilized by UV-crosslinking. [49] Meanwhile, the visible light-induced crosslinking using a ruthenium-initiated chemistry has been investigated in tissue engineering. Moreover, UV light irradiation can influence chromosomal and genetic instability in cells and visible light can penetrate to a greater depth for thick constructs. [50] Previously, Lim and coworkers reported the utility and the potential of visible light-induced hydrogelation using ruthenium II trisbipyridyl chloride ($[\text{Ru}(\text{bpy})_3]^{2+}$) and sodium persulfate (SPS) were demonstrated. In the system, phenolic hydroxyl groups in the amino acid residues such as tyrosine are able to crosslink to form the gelation *via* light irradiation. [51] Elvin and coworkers reported a highly elastic tissue sealant and studied cytotoxicity of ruthenium catalyst and initiators as $[\text{RuII}(\text{bpy})_3]^{2+}$ and sodium persulfate (SPS) in **Figure 1.11**. The results showed that ruthenium catalyst and SPS were not

toxic to cells at concentration of 1 mM and 0.3 mM. However, SPS was rapidly consumed during the photochemical crosslinking reaction until the concentration was less than 20 mM that were not toxic to L929 fibroblast cells. [52]

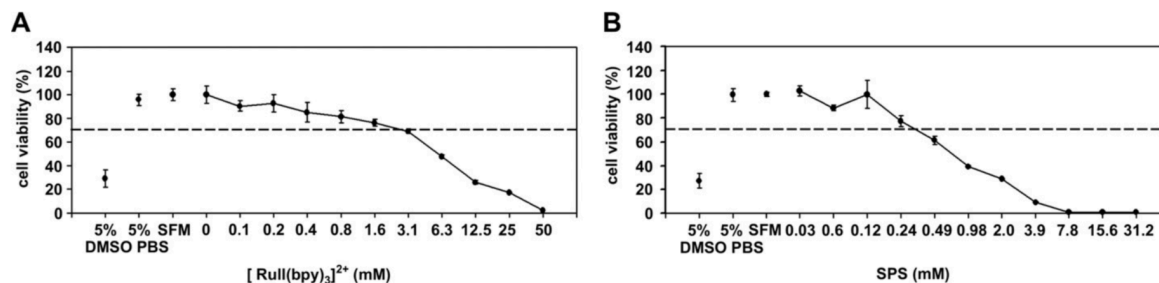


Figure 1.11 Toxicity of individual components to L929 mouse fibroblast cells *in vitro*. Components that reduced cell viability to less than 70% (dashed line) were deemed cytotoxic. Negative controls: PBS and Serum-Free Media (SFM). Positive control: 5% DMSO in PBS. A) Cytotoxicity of [RuII(bpy)₃]²⁺. B) Cytotoxicity of SPS. [52]

Moreover, on tissue surface, there are many amino acids including tyrosine. The tyrosine on tissue surface can also crosslink by ruthenium catalyst and SPS to provide chemical covalent bonding from tyrosine into di-tyrosine for enhance adhesion at interface as shown in

Figure 1.12

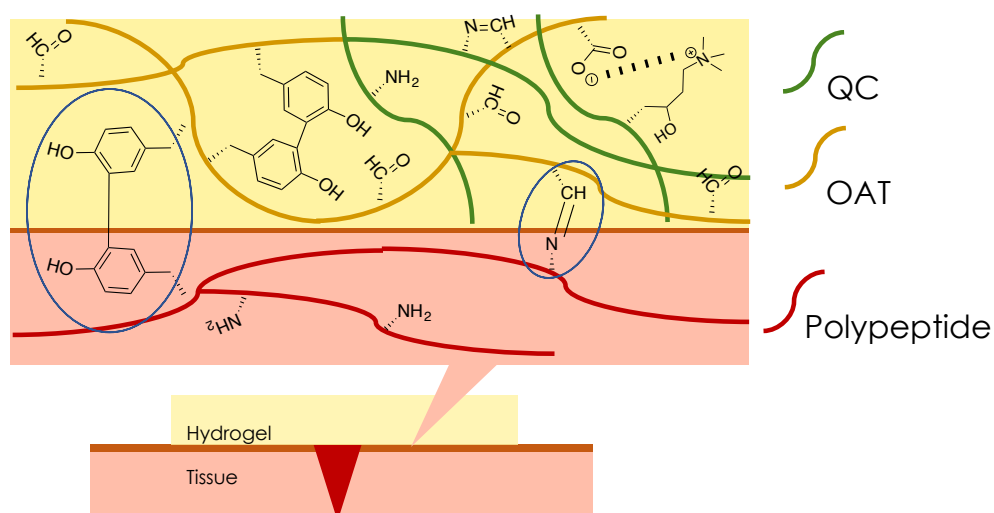


Figure 1.12 Schematic representation of adhesion bonding between polysaccharide-based hydrogel and tissue surface.

1.3 OBJECTIVES

Part 1: Polyphosphoester-based hydrogel

1. To synthesize and characterize IPP and P-TMP monomers
2. To synthesize and characterize poly(IPP-*r*-TMP) *via* ROP
3. To form hydrogel *via* visible photo-crosslinking

Part 2: Polysaccharide-based hydrogel

1. To synthesize and characterize oxidized alginate-tyrosine (OAT) *via* EDC/NHS coupling and oxidation reaction
2. To synthesize and characterize quaternized chitosan (QC) *via* nucleophilic substitution with glycidyltrimethylammonium chloride (GTMAC).
3. To prepare and characterize the hydrogel formed *via* gelation of OAT and QC.

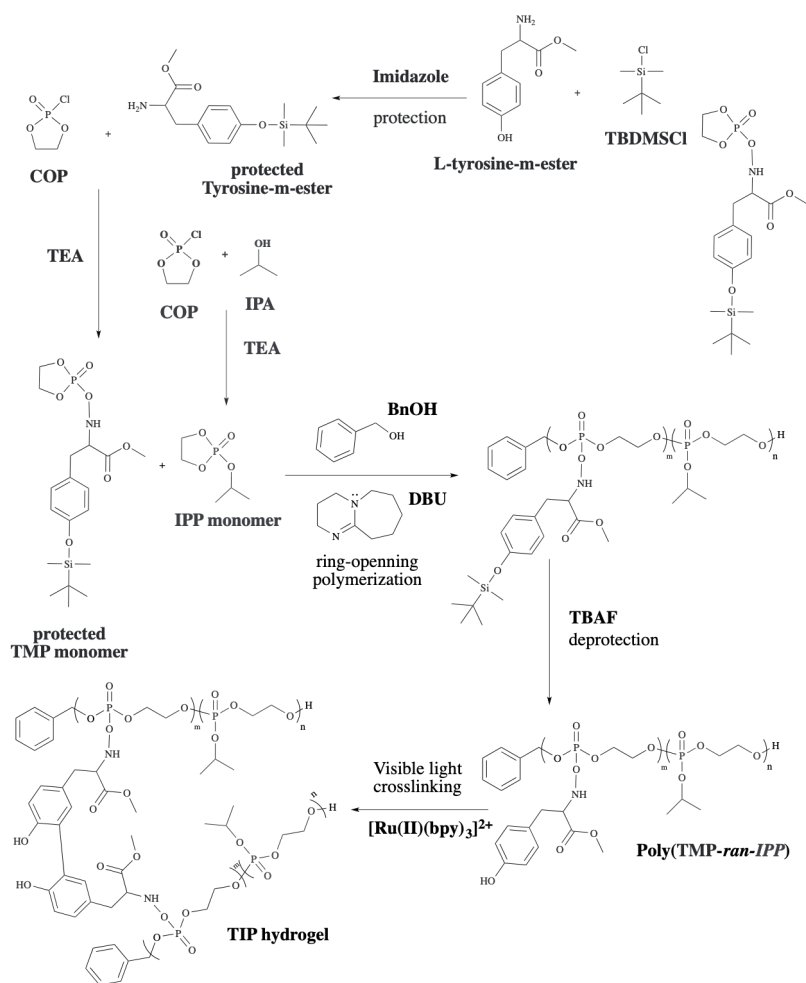
CHAPTER 2

EXPERIMENTAL METHOD

2.1 Instruments

1. Balances (Precisa, Model XT220A, Switzerland)
2. Hot plate-stirrer (IKA, Model C-MAG HS 7, Germany)
3. Freeze dryer (LABCONCO, Model 77535-01, USA)
4. Nuclear magnetic resonance spectrometer (JEOL, JNM-ECZR 500 MHz, USA)
5. Infrared spectrometer (FTIR) (Nicolet Impact 6700 FT-IR, USA)
6. UV-Visible Spectrophotometer (Agilent, HP 8453, USA)

2.2 Polyphosphoester-based hydrogel

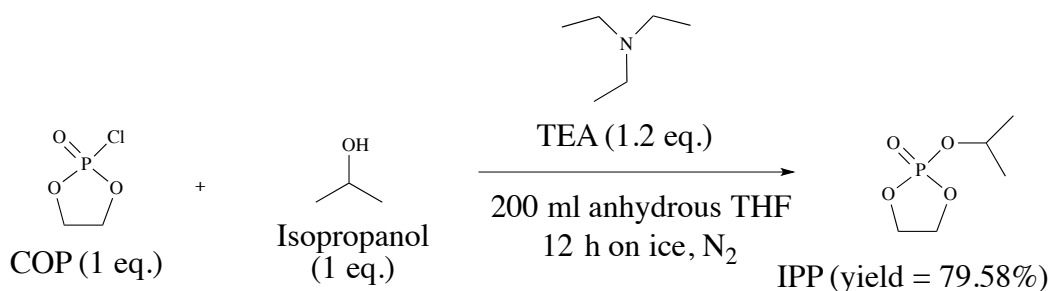


Scheme 2.1 Synthesis overview of polyphosphoester-based hydrogel.

2.2.1 Materials

2-Chloro-1,3,2-dioxaphospholane-2-oxide (COP), triethylamine (TEA), *L*-tyrosine-methyl-ester hydrochloride (L-tyr), imidazole and *tert*-butyldimethylsilyl chloride (TBDMSCl) were purchased from Tokyo Chemical Industry Co., Ltd. 2-Propanol (IPA) and anhydrous tetrahydrofuran (THF) were purchased from Sigma-Aldrich. Sodium sulfate (Na₂SO₄) and dichloromethane (DCM) were purchased from Carlo Erba Reagents. DCM was dried over calcium hydride and refluxed under a nitrogen (N₂) atmosphere prior to use. Sodium chloride was purchased from Merck KGaA. Ethyl acetate (EtOAc) and hexane were supplied from RCI Labscan.

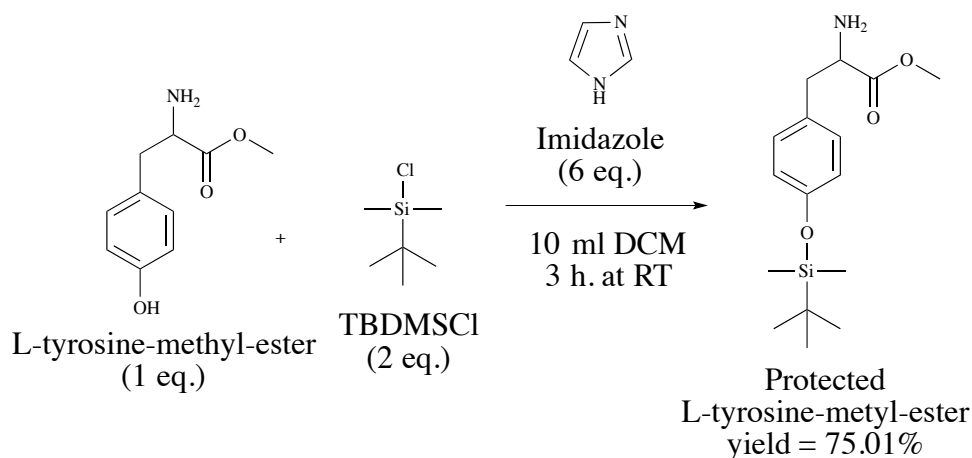
2.2.2 Synthesis of 2-isopropoxy-1,3,2-dioxaphospholane 2-oxide (IPP) monomer



Scheme 2.2 Synthesis of IPP monomer.

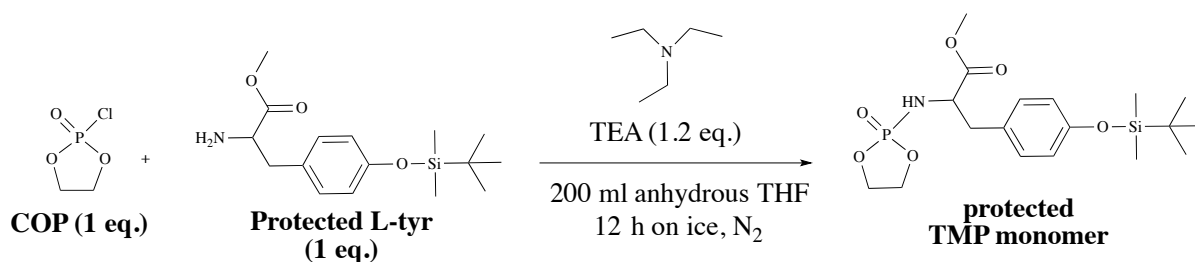
Firstly, IPP monomer was prepared according to a modified version of a previously published method [21, 53]. IPA (6.37 g, 106 mmol, 1 eq) and TEA (12.87 g, 127 mmol, 1.2 eq) were dissolved and stirred in 180 mL of anhydrous THF in an ice bath. Then, COP (15.01 g, 106 mmol, 1 eq) in 20 mL of anhydrous THF was dropwise added into the mixture under N₂ atmosphere for 12 h. The mixture was stirred on ice bath for 2 h and at ambient temperature for 10 h. After 12 h, the mixture was filtered by vacuum filtration to remove ammonium salt as by-product (white solid) and the product was washed with THF. After that, THF was removed by rotatory evaporator. IPP was purified by vacuum distillation with 80% yield, as clear liquid and the monomer was characterized by ¹H-NMR spectroscopy.

2.2.3 Synthesis of methyl-3-(4-((tert-butyldimethylsilyl)oxy)phenyl)-2-(((2-oxido-1,3,2-dioxaphospholan-2-yl)oxy)amino)propanoate, protected *N*-tyrosine-*m*-ester phospholane amidate (P-TMP) monomer



Scheme 2.3 Synthesis of protected L-tyrosine methyl ester.

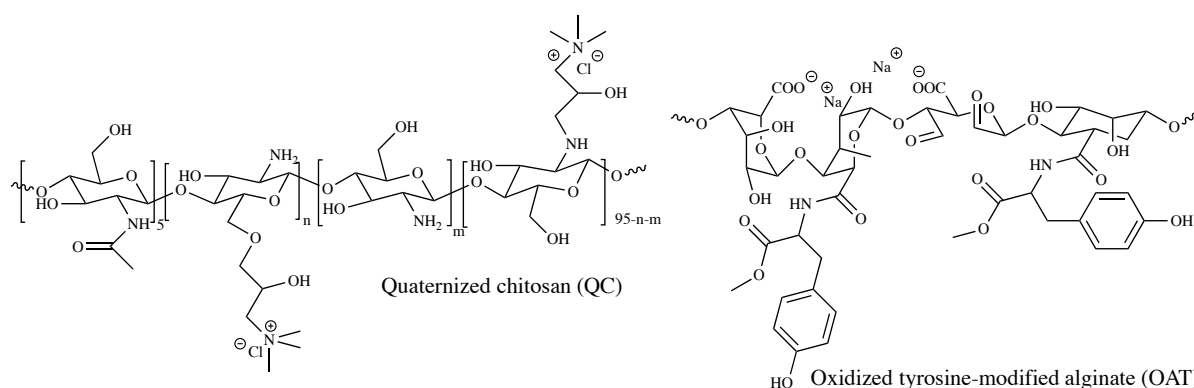
To synthesize P-TMP monomer, the phenolic hydroxyl group on L-tyrosine-methyl-ester was protected by TBDMSCl reagent following the previous work [54]. Briefly, the L-tyr (695.0 mg, 3 mmol, 1 eq), imidazole (1.021 g, 18 mmol, 6 eq) and TBDMSCl reagent (904.3 mg, 6 mmol, 2 eq) were stirred in 10 mL of distilled DCM under N₂ atmosphere at ambient temperature. After 3 h, 30 mL of DCM and 50 mL of DI water were added into the mixture for extraction. The organic phase was collected and extracted with DI water 2 times. After that, the organic phase was further extracted with 50 mL of brine and added with Na₂SO₄ to remove trace amount of water. DCM was then eliminated by rotatory evaporator and the product was confirmed by TLC. The concentrated product (protected Tyrosine-*m*-ester, P-tyr-*m*-ester) was separated by silica gel column chromatography (mobile phase 4:6 EtOAc:Hexane) with 75% yield as pale yellow liquid. Finally, the product was characterized by ¹H-NMR and ATR-FTIR spectroscopy.



Scheme 2.4 Synthesis of P-TMP monomer.

Then, P-TMP monomer, which was synthesized following the modified procedure of phospholane monomers [55], was prepared using a mixture of P-tyr-m-ester (2.6917 g, 8.70 mmol, 1 eq) and TEA (1.0560 g or 1.46 ml, 127 mmol, 1.2 eq), which were dissolved and stirred in 30 mL of anhydrous THF in an ice bath. Then, COP (1.239 g, 8.70 mmol, 1 eq) in 20 mL of anhydrous THF was dropwise added into the mixture under N₂ atmosphere for 12 h. The mixture was stirred on ice bath for 2 h at ambient temperature for 10 h. After 12 h, the mixture was filtered by vacuum filtration to remove ammonium salt as by-product (white solid) and washed with THF. After complete conversion of COP, as confirmed by TLC, the reaction mixture was filtered, and the filtrate was concentrated. The concentrated filtrate was purified by column chromatography using silica gel as stationary phase and ethyl acetate as an eluent giving pale-yellow liquid. Finally, the product was characterized by ¹H-NMR, ³¹P-NMR and FT-IR spectroscopy.

2.3 Polysaccharide-based hydrogel



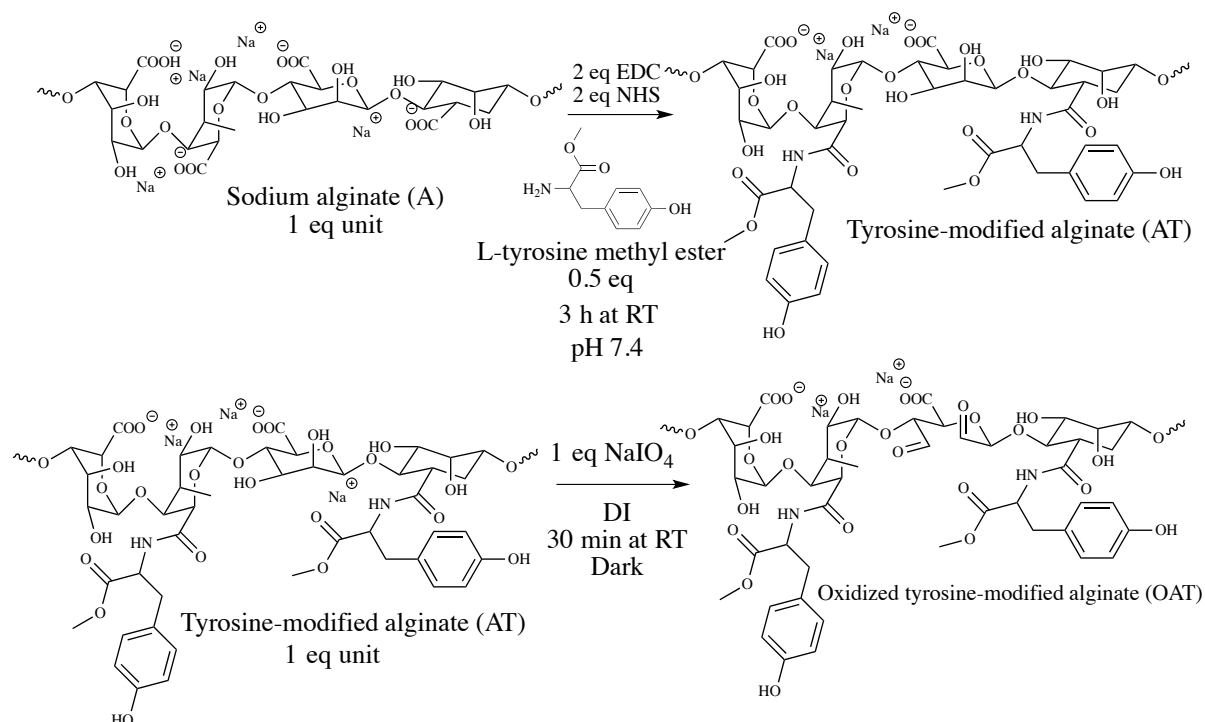
Scheme 2.5 Structures of quaternized chitosan and oxidized tyrosine-modified alginate to be used for hydrogelation *via* Schiff base linkage.

2.3.1 Materials

Alginate sodium salt (viscosity of 2% solution at 25 °C : 250 cps), L-tyrosine-methyl-ester hydrochloride (L-tyr), 1-ethyl-3-(3-dimethylaminopropyl)carbodiimide hydrochloride (EDC.HCl), *N*-hydroxysuccinimide (NHS), and glycidyltrimethylammonium chloride (GTMAC) were purchased from Sigma-Aldrich. Chitosan (DD = 95% and M_w = 100,000 Da) was purchased from Seafresh Chitosan (LAB). Trifluoroacetic acid was purchased

from Honeywell International Inc. Sodium chloride (NaCl) and acetic acid were purchased from Merck KGaA. Sodium metaperiodate was purchased from Kemaus, Molecule. Tris(bipyridine)ruthenium(II) chloride ($[\text{Ru}(\text{bpy})_3]\text{Cl}_2$, 98%) and sodium persulfate (SPS, 98%) were purchased from Acros Organics B.V.B.A.

2.3.2 Synthesis of tyrosine-modified alginate (AT)



Scheme 2.6 Synthesis of oxidized tyrosine-modified alginate in 2 reaction steps.

Firstly, alginate has to be modified with tyrosine before oxidation step to prevent Schiff-base linkage between aldehyde groups on alginate and primary amine on tyrosine. Tyrosine-modified alginate was synthesized *via* amidation using a modified procedure. [56] Briefly, an 1% (w/v) solution of sodium alginate in 25 mL phosphate-buffered saline (PBS) pH 7.4 was prepared. Then, 443.6 mg of EDC.HCl and 266.3 mg of NHS were added to the mixture to activate the carboxylic acid groups of the alginate. After 5 min, 134.0 mg of L-tyr (molar ratio of NHS:EDC:L-tyr:alg unit 2:2:0.5:1) was added to the solution. And the reaction proceeded at room temperature for a predetermined period of time (1, 3, 6, 9, 12 and 24 h). After that, the tyrosine-modified alginates were purified by dialysis against 100 mM NaCl, 30% EtOH, and

DI water (MWCO 3500; SnakeSkin™, Thermo Scientific, USA for 1, and 2 days, respectively and lyophilized to obtain solid-like white cotton. The product was finally characterized by ATR-FTIR spectroscopy and UV-Visible spectrophotometer. The amount of L-tyr (0.5, 1.0, 1.5, and 2.0 eq) was also varied to determine its effect of the degree of L-tyr substitution.

2.3.3 Gelation by visible light-induced crosslinking

Visible light-induced crosslinking was performed following a previous work. [52] Stock solutions of 50 mM $[\text{RuII}(\text{bpy})_3]^{2+}$ and 1 M SPS was then prepared in aqueous media. Mixture of 1% of AT with different % of tyrosine, 1 mM $[\text{RuII}(\text{bpy})_3]^{2+}$ and 20 mM SPS in PBS, pH 7.4 were dispersed in 3 mL vial, and the mixture was irradiated for 30 s at room temperature by Cool Daylight lamp (Helix 42W) with a distance of 3 cm.

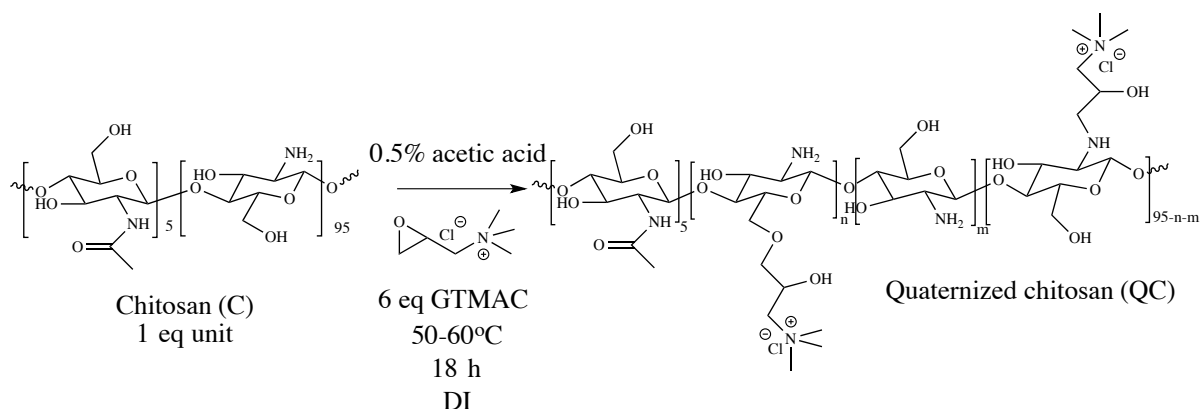
2.3.4 Synthesis of oxidized tyrosine-modified alginates (OAT)

Tyrosine-modified alginate was oxidized following a previously reported procedure [35]. Tyrosine-modified alginate was dissolved in 50 mL Milli-Q water to prepare 1% (w/v) solution and added with 500 mg of sodium periodate (1:1 mass ratio). The mixture solution was then stirred at room temperature for 30 min and kept out of the light. After that, 5 mL ethylene glycol was added to terminate the reaction. The mixture solution was dialyzed (MWCO = 3,500) for 3 days against DI water, lyophilized to obtain the final product with 80% yield as white cotton. The product was characterized by FT-IR technique and 2,4-dinitrophenylhydrazine (DNP) test.

2.3.5 Determination of degree of tyrosine substitution on tyrosine-modified alginates

Determination of degree of tyrosine substitution was based on the measurement of phenolic hydroxyl groups on alginate backbone by UV-Visible spectrophotometer at 280 nm using PBS buffer pH 7.4 as a blank. Firstly, standard calibration curve of L-tyrosine methyl ester.HCl was established in a range of 0.01-10 mM. Then 2.5 mg of tyrosine-modified alginates was dissolved in 1.0 mL of pH 7.4 PBS buffer to prepare 0.25% (w/v) solution as stock solution. The solution was then measured for its absorbance and the amount of tyrosine can be determined from the calibration curve.

2.3.6 Synthesis of quaternized chitosan (QC)



Scheme 2.7 Synthesis of quaternized chitosan.

Quaternized chitosan was synthesized as reported in a previous work. [57] Briefly, 0.5 g of chitosan powder was suspended in 19 mL DI water, and then 0.2 mL of acetic acid (*i.e.* ~0.5% v/v) was added. [58] The mixture was stirred for 30 min prior to a dropwise addition of GTMAC with continuous stirring. The mole ratio of GTMAC to chitosan unit was fixed at 6:1 to produce QC. The reaction mixture was stirred at 100 rpm at 50-60 °C for 18 h. Following the reaction, the undissolved polymer was removed by centrifugation of the mixture at 6000 rpm for 5 min at ambient temperature. For purification, the solution was filtered, methanol was added to remove the excess GTMAC, and the QC was precipitated in acetone. The purification process was repeated three times, and the purified QC was dried in a vacuum oven at 25 °C for 5 days with subsequent grinding of the product to obtain fine powder.

CHAPTER 3

RESULTS AND DISCUSSION

3.1 Polyphosphoester-based hydrogel

3.1.1 Synthesis of 2-isopropoxy-1,3,2-dioxaphospholane 2-oxide (IPP) monomer

The IPP monomer was synthesized *via* nucleophilic substitution of COP and IPA using TEA as catalyst and anhydrous THF as solvent to avoid violent reaction between COP and moisture. The monomer was then filtered to eliminate by-products and was purified by vacuum distillation to give the product with 80% yield. According to $^1\text{H-NMR}$ spectra of IPP and COP (Figure 3.1), methylene protons of COP appear in the range of 4.2 - 4.5 ppm ($\text{H}_{\text{A, B}}$), while chemical shifts at 1.3 (H_{D}), and 4.7 (H_{C}) ppm can be attributed to the isopropyl protons of IPP. Thus, it can be confirmed that IPP monomer was successfully synthesized and purified.

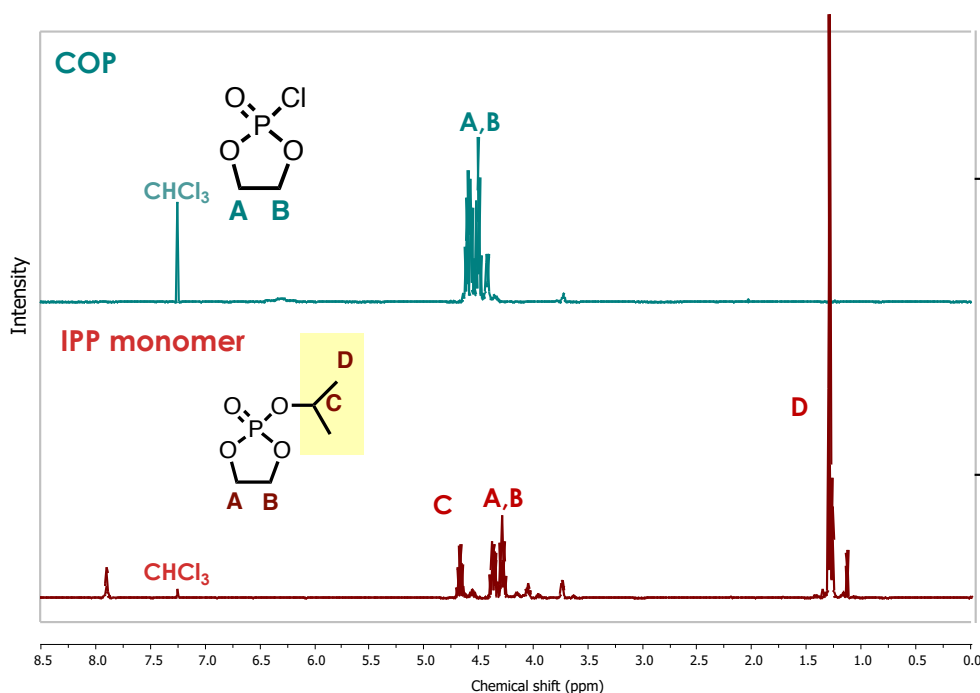


Figure 3.1 $^1\text{H-NMR}$ spectra of COP precursor and IPP monomer in CDCl_3 .

3.1.2 Synthesis of methyl-3-(4-((tert-butyldimethylsilyl)oxy)phenyl)-2-(((2-oxido-1,3,2-dioxaphospholan-2-yl)oxy)amino)propanoate, protected *N*-tyrosine-m-ester phospholane amidate (P-TMP) monomer

To synthesize P-TMP monomer, the phenolic hydroxyl groups on L-tyrosine-methyl-ester had to be specifically protected by TBDMSCl reagent because L-tyrosine-methyl-ester contains 2 nucleophilic groups as phenolic hydroxyl group and amino group. TBDMSCl was used for preventing *O*-attack to COP in P-TMP monomer synthesis and the remaining amine would be allowed to react with COP in the next step. After polymerization and deprotection step, phenolic hydroxyl moieties play a crucial role in the crosslinking step *via* visible light irradiation with ruthenium catalyst.

After being synthesized and purified, the resulting protected L-tyrosine methyl ester was characterized by FT-IR spectroscopy. As depicted in **Figure 3.2**, FT-IR spectra demonstrated characteristic signals of Si-C stretching at 780 and 836 cm^{-1} . Moreover, the product was characterized by $^1\text{H-NMR}$ spectroscopy. Signals at chemical shift of 0.21 ppm (H_A) and 0.98 ppm (H_B) of silyl groups and proton of tyrosine methyl ester (H_C) shifted from 4.25 to 3.66 ppm because of different solvents were used for analysis as shown in **Figure 3.3**. Thus, these results confirmed that the protected L-tyrosine methyl ester was successfully synthesized and purified by this method.

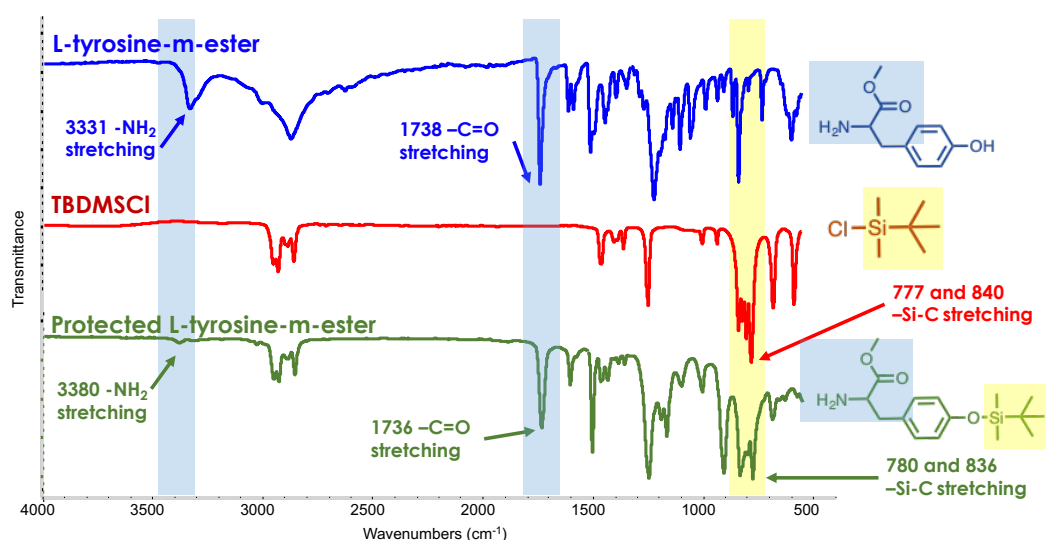


Figure 3.2 FT-IR spectra of L-tyrosine methyl ester, TBDMSCl and protected L-tyrosine methyl ester.

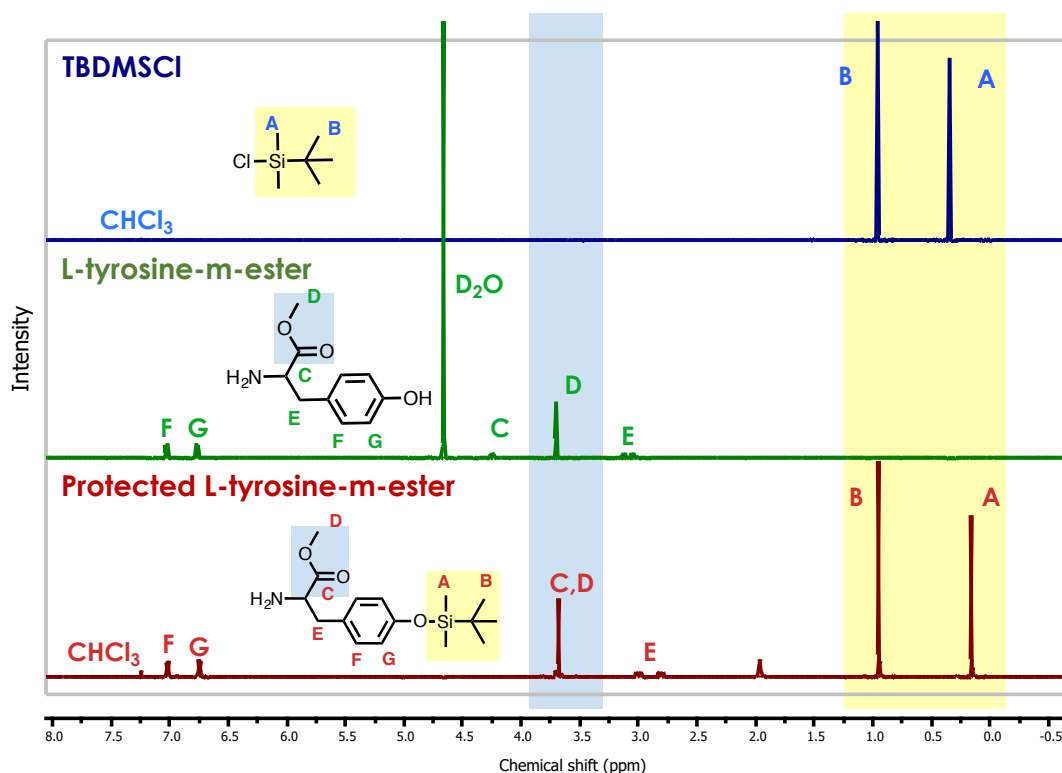


Figure 3.3 ¹H-NMR spectra of L-tyrosine methyl ester in D₂O, TBDMSCl and protected L-tyrosine methyl ester in CDCl₃.

After *O*-nucleophile protection of tyrosine methyl ester, the protected product was used as *N*-nucleophile that was expected to substitute chlorine atom on COP *via* nucleophilic substitution reaction. After the reaction, concentrated filtrate of the monomer was purified by column chromatography such as flash column and silica gel plug instead of vacuum distillation. The cyclic structure of protected *N*-tyrosine-m-ester phospholane amidate (P-TMP) monomer is vulnerable to be broken at high temperature so that distillation cannot be used for purification. Firstly, crude P-TMP monomer of the first batch was purified by flash column chromatography using ethyl acetate (EtOAc) and 1% triethylamine (TEA) as mobile phase. TEA was used for neutralizing the silica gel because acidity of silanol groups may affect ring-opening of the cyclic phospholane. Unfortunately, the result after separation (second to fourth fractions were collected) showed that the reactant, P-tyrosine-m-ester, was observed by TLC and ³¹P NMR spectroscopy indicating that no product occurred. (**Figure 3.4**)

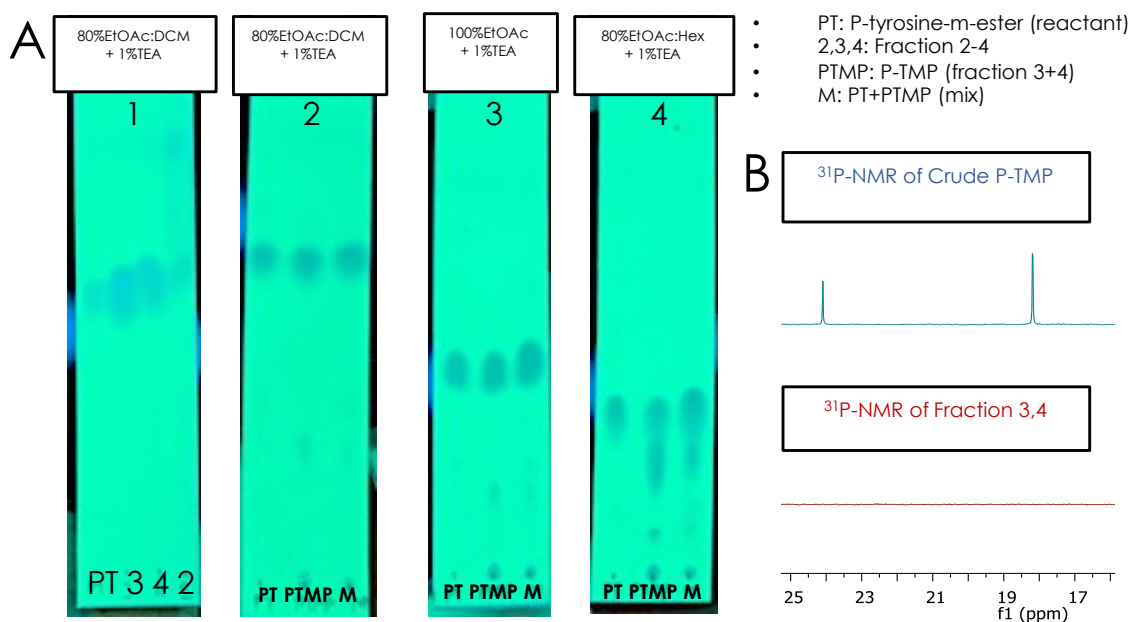


Figure 3.4 A) TLC results of standard PT, fraction, separated product in different mobile phase and B) ³¹P-NMR spectra of crude product and separated product.

In different mobile phase (**Figure 3.4A**), all TLC spots of products that appear at the same position as PT (reactant). Thus, we hypothesized that both P-TMP synthetic route or the purification method were not effective. Thus, to prove the hypothesis, crude product of P-TMP monomer was characterized by ³¹P-NMR spectroscopy. There were both phospholane amidate at 24 ppm (*N*-attack) and phosphate phospholane at 18 ppm (*O*-attack) signals but the amidate intensity was lower than that of phosphate phospholane, indicating that the product could not be separated by this method. Moreover, ³¹P-NMR spectrum of fraction 3-4 show no signal (**Figure 3.4B**), implying that the method was not suitable for this reaction. We proposed that sensitive P-TMP might be decomposed and hydrolyzed in silica gel column. According to ¹H-NMR spectrum of fraction 3-4 in **Figure 3.5**, the obtained product was P-tyrosine-m-ester which came from hydrolysis of P-TMP.

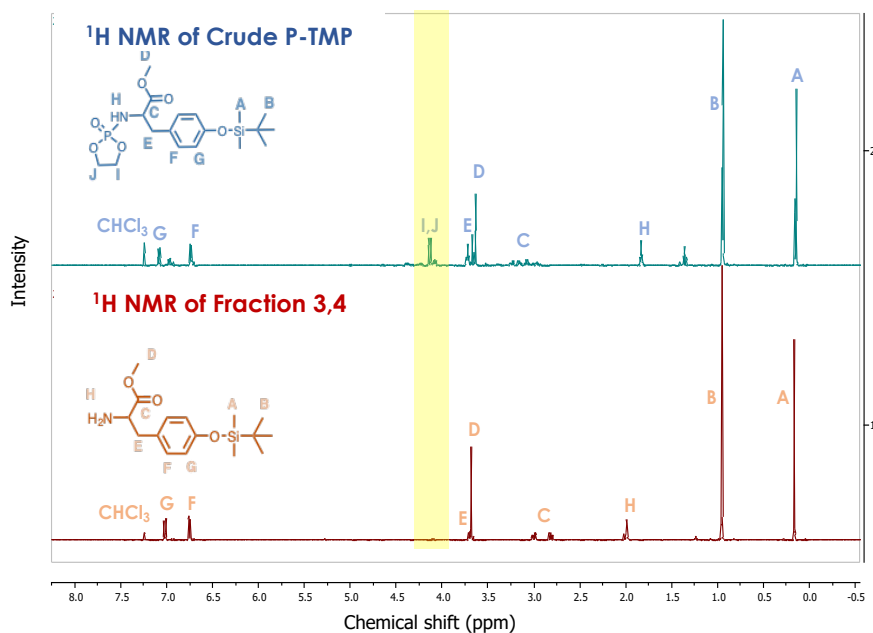


Figure 3.5 $^1\text{H-NMR}$ spectra of crude product and fraction 3, 4 in CDCl_3 .

The second batch of P-TMP monomer was synthesized again and crude P-TMP was checked with $^{31}\text{P-NMR}$ spectroscopy. According to the results, P-TMP was the major product but there was an impurity (18 ppm) of *O*-attacked phospholane as demonstrated in **Figure 3.6B**. To avoid the problem due to monomer decomposition, a very fast method as silica gel plug [59] was selected to separate P-TMP monomer. A set-up is shown in **Figure 3.7A**

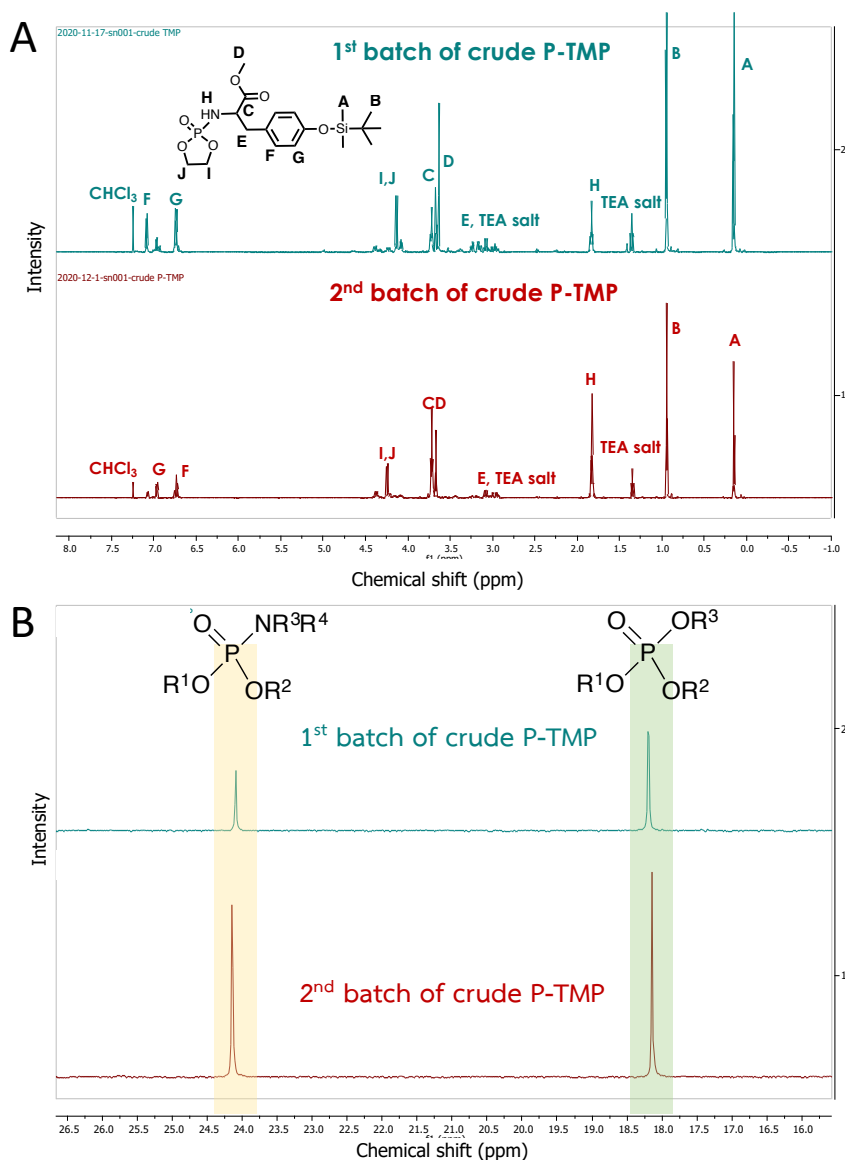


Figure 3.6 A) ¹H-NMR and B) ³¹P-NMR spectra of crude product of the first and second batches.

In **Figure 3.7B**, the crude P-TMP monomer was separated into 3 spots observed on TLC plate (4:1 THF:hexane was used as mobile phase). The first spot (from top) was protected tyrosine (PT), indicating that the substrate did not completely convert to the product. We proposed that the second one was P-TMP monomer because it shows higher polarity. The last one was probably all ring-opened compounds and by products.

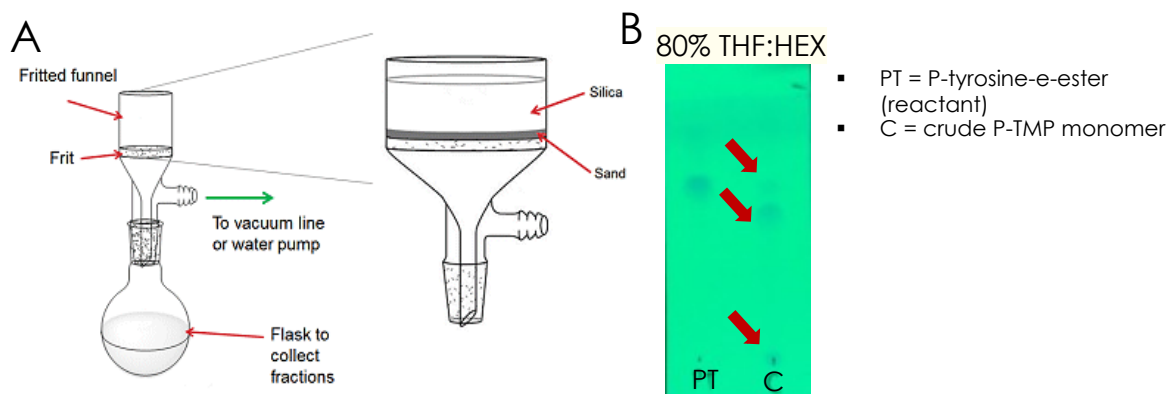


Figure 3.7 A) A setup of instrument used for silica gel plug method B) TLC spots of standard PT and crude product.

After separation, fraction 1–3 were obtained and checked by TLC. The TLC still showed 3 spots (**Figure 3.8**). From this result, the TLC did not match for following separation process. Then, fraction 1–3 were characterized by ^{31}P -NMR and integration of each peaks were calculated as PA/PP ratio to determine ratio between phospholane amidate at 24 ppm (*N*-attack) and phosphate phospholane at 18 ppm (*O*-attack) (**Figure 3.9**). Besides, the result showed that all of fractions had low PA/PP ratio meaning that the product could not be separated by this method. We proposed that P-TMP monomer may react with moisture in the air or silanol groups on silica surface in the column, resulting in ring-opened phosphoester. Possible products that could occur were summarized in **Figure 3.10**.

In conclusion, P-TMP monomer could be synthesized by this method with low yield but it could not be purified by flash column chromatography and silica gel plug methods. Thus, a suitable synthetic and purifying procedure need to be optimized in order to avoid decomposition of sensitive P-TMP monomer.

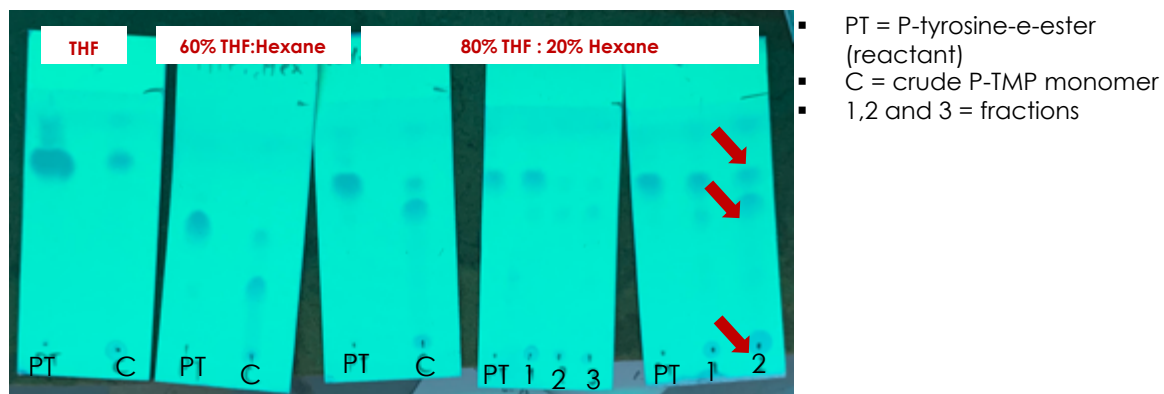
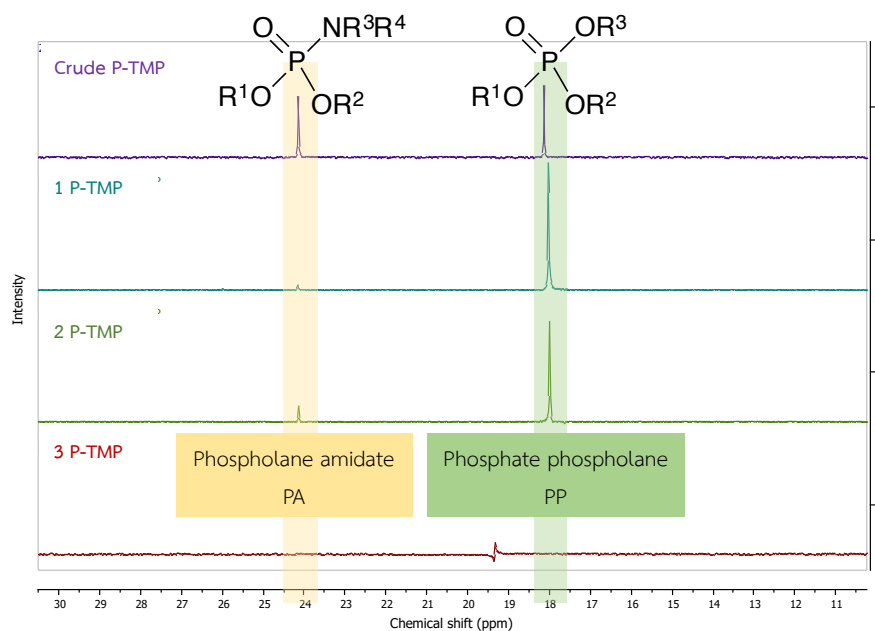


Figure 3.8 TLC spots of standard PT, crude product and fractions.



PA/PP integration ratio calculated from ^{31}P -NMR

- Crude P-TMP = crude of protected TMP monomer: $1/0.84 = 1.19$
- 1 P-TMP = first fraction: $1/32.16 = 0.03$
- 2 P-TMP = second fraction: $1/6.38 = 0.16$
- 3 P-TMP = third fraction: no signal

Figure 3.9 ^{31}P -NMR spectra of crude product and fraction 1, 2 and 3 and PA/PP ratio.

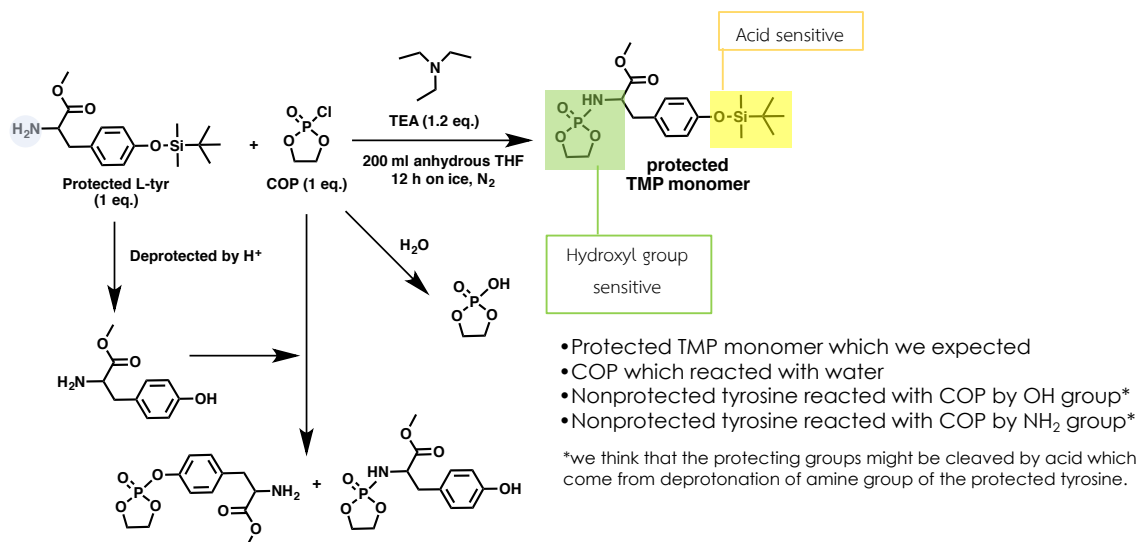


Figure 3.10 The possible products in the reaction and purification methods.

3.2 Polysaccharide-based hydrogel

3.2.1 Synthesis of oxidized tyrosine-modified alginate (OAT)

To synthesize oxidized tyrosine-modified alginate, tyrosine-modified alginate (AT) was synthesized by coupling reaction between carboxylic groups on alginate units and primary amine groups on L-tyr and using EDC/NHS to activate carboxylic groups to improve reactivity between carboxylic groups and amine groups. Phenolic groups of AT enable covalent photocrosslinking between adjacent polysaccharide chains in aqueous solutions, forming hydrogel. AT synthetic conditions were optimized by varying reaction time and feed mole ratio of L-tyr to alginate units. FTIR spectral analysis shown in **Figure 3.11A** revealed the characteristic signals of unmodified sodium alginate at 3386 cm^{-1} (O-H stretching), 2925 cm^{-1} (C-H stretching), 1581 cm^{-1} (C=O stretching), and 1414 cm^{-1} (O-H bending). The emergence of ester (C=O stretching) signal at 1730 cm^{-1} in FTIR spectrum of AT (**Figure 3.11B**) verifying the success of L-tyr modification. Nevertheless, carbonyl groups of amide (C=O stretching) at approximately 1600 cm^{-1} cannot be obviously observed because of overlapping with C=O stretching signal of alginate. As tyrosine can absorb UV wavelength at 280 nm, the absorption of AT confirmed the presence of tyrosine in its structure (**Figure 3.12**) by using PBS buffer pH 7.4 as blank.

To provide Schiff-base linkage with chitosan, AT was further oxidized by NaIO₄ with 1:1 mole ratio. The oxidized product presents higher solubility in aqueous media (**Figure**

3.13A) because dialdehyde structures on the alginate backbone decrease hydrogen bonding among polymer chains. FT-IR spectrum (**Figure 3.11C**) of the oxidized product, OAT shows a band of the carbonyl (C=O stretching) for aldehyde on alginate backbone at 1715 cm^{-1} albeit its low intensity. Thus, 2,4-DNP reagent was used to evaluate whether alcohol groups in pyranose ring could be oxidized into aldehyde groups. Yellow-orange precipitates of dinitrophenylhydrazone was observed as a positive test indicating the presence of aldehyde groups in OAT (**Figure 3.13B**). Therefore, OAT was successfully synthesized by oxidation reaction.

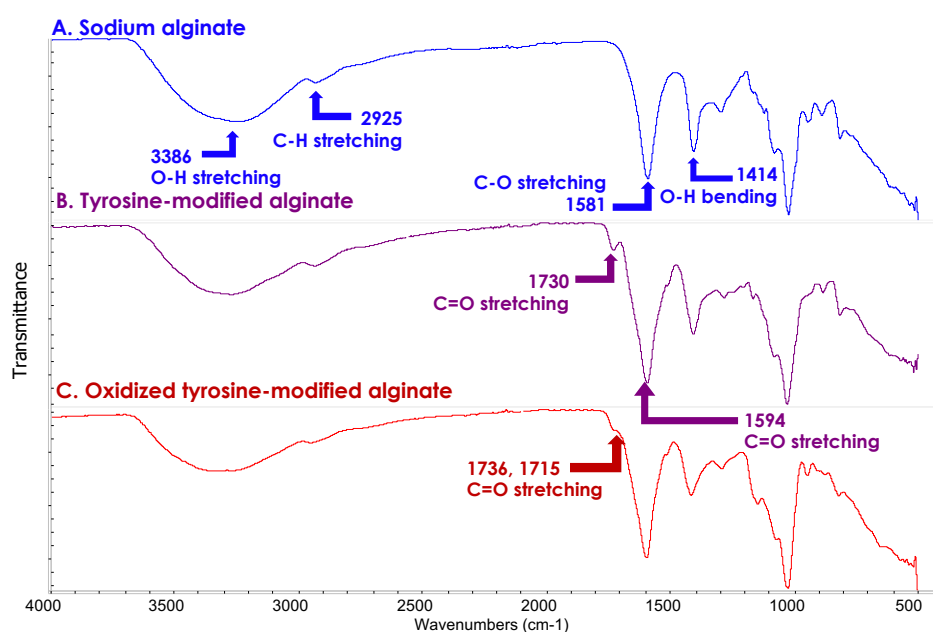


Figure 3.11 FT-IR spectra of A) sodium alginate, B) tyrosine-modified alginate and C) oxidized tyrosine-modified alginate.

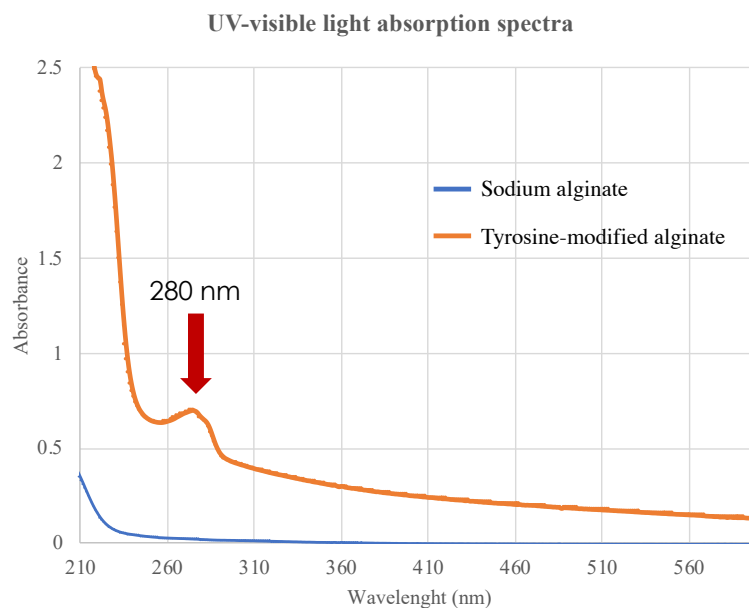


Figure 3.12 Absorption spectra of sodium alginate compared with tyrosine-modified alginate.

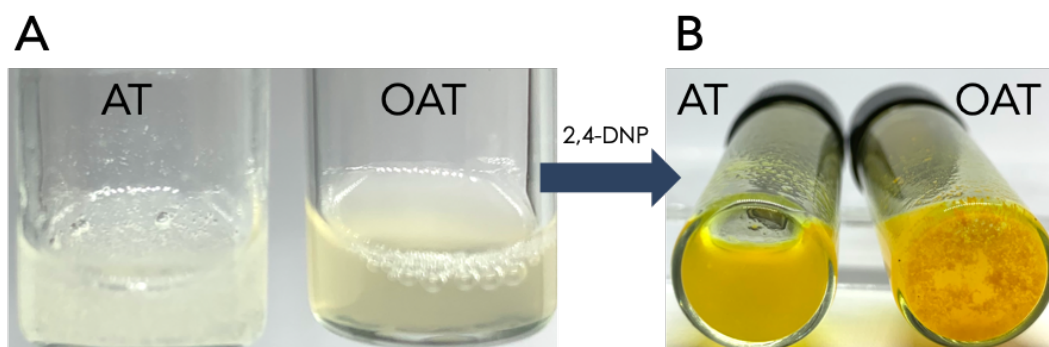


Figure 3.13 Appearance of A) tyrosine-modified alginate (AT) and oxidized tyrosine-modified alginate (OAT) in aqueous media and B) 2,4-DNP test results of AT and OAT.

In order to determine degree of tyrosine substitution (%DS) in the product by using UV-Visible spectrophotometer, a calibration curve of standard tyrosine methyl ester in a concentration range of 0.01-10 mM was first established as shown in **Figure 3.14**. A linear equation was evaluated as $y = 1.272x + 0.0061$ with acceptable $R^2 = 0.9998$.

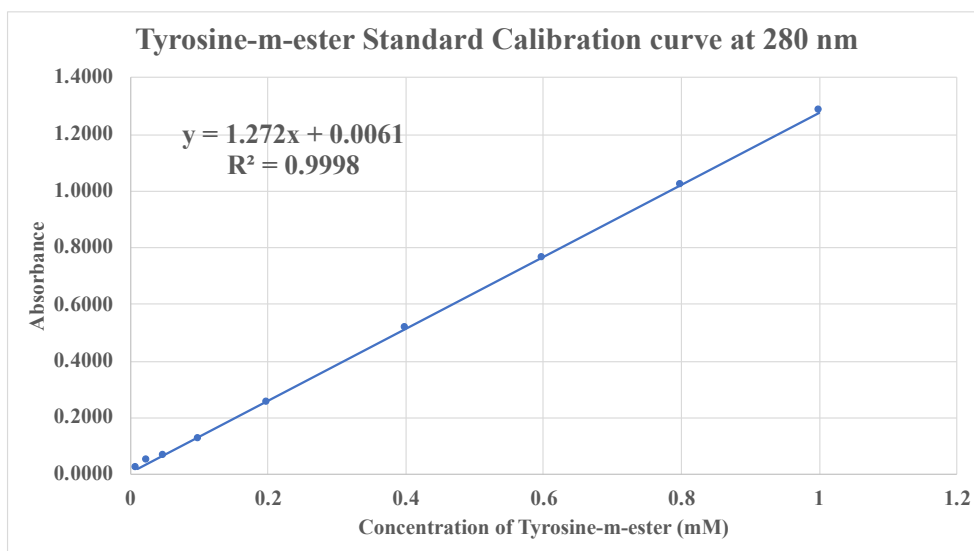


Figure 3.14 Standard calibration curve of tyrosine-m-ester concentration (0.01-1.0 mM).

Effect of reaction time and feeding mole ratio of L-tyr on %DS of tyrosine in AT products were investigated. Firstly, AT was synthesized by varying reaction time (1, 3, 6, 9, 12 and 24 h) and the kinetic plot was demonstrated in **Figure 3.15**. The %DS of tyrosine dramatically increased in the first 1 h, reaching 13.77% tyrosine. Then, it slightly rose until 3 h, representing 14.63% and the %DS of tyrosine did not significantly change with extension of the reaction time. So, the coupling reaction of sodium alginate with tyrosine methyl ester was basically completed in 3 h, indicating that this period of time was sufficient for the generation of the highest degree of tyrosine substitution.

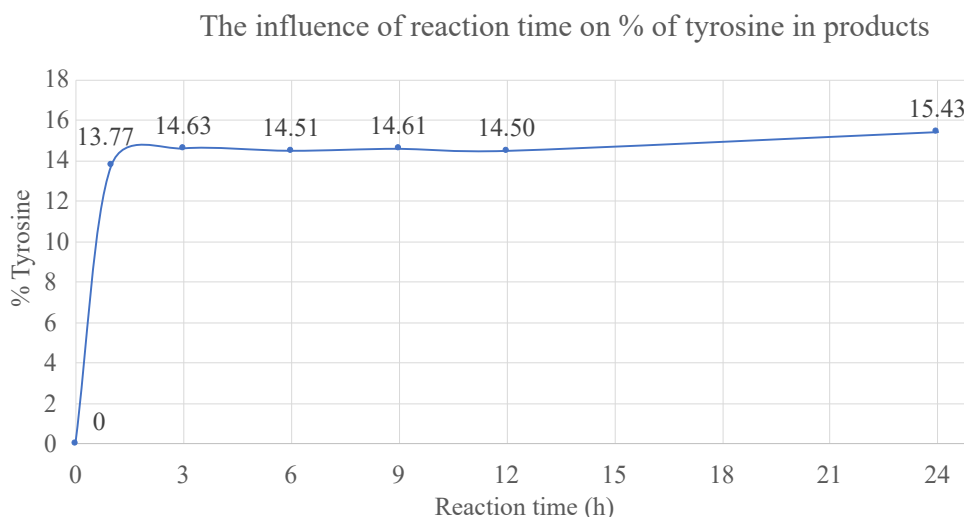


Figure 3.15 Degree of tyrosine substitution (%DS) in AT versus reaction time.

With reaction time of 3 h, equivalent of tyrosine methyl ester was varied (0.5, 1.0, 1.5, 3.0 eq). It was found that %DS in each sample increases with increasing feeding mole ratio of tyrosine methyl ester (**Table 3.1**). Unfortunately, by increasing % tyrosine in the samples, the solubility in PBS buffer (pH 7.4) decreases. For example, 3% w/v of all samples could not dissolve in an aqueous media homogeneously, 2% w/v of only AT1 and AT2, which has lower %tyrosine (less than 20%) could well dissolve, and 1%w/v of all samples were soluble in the aqueous media. This is because of interactions between polymer chain such as hydrogen bonding, polar-polar force, Van der Waals forces, static electric force, and also π - π interactions. The aromatic groups of tyrosine introduced to the AT would increase its hydrophobicity so thus decreases its aqueous solubility.

Moreover, gel formation of AT was tested as compared with the unmodified sodium alginate *via* the reaction between Ru(III) and persulfate (**Figure 3.16**). In the presence of persulfate with visible light, Ru(III) and sulfate radical are produced from photolyzed $[\text{Ru(II)(bpy)}_3]^{2+}$. Ru(III), which is a potent single-electron oxidant, would oxidize residues such as tyrosine molecule. The radical could subsequently form crosslinked networks. [60] According to the gelation results (**Figure 3.17**), all of 1%w/v AT samples could form hydrogel upon photoirradiation within 30 s while the unmodified sodium alginate could not form gel. Therefore, AT1 sample was chosen to be further studied because of its great solubility and gelation performance.

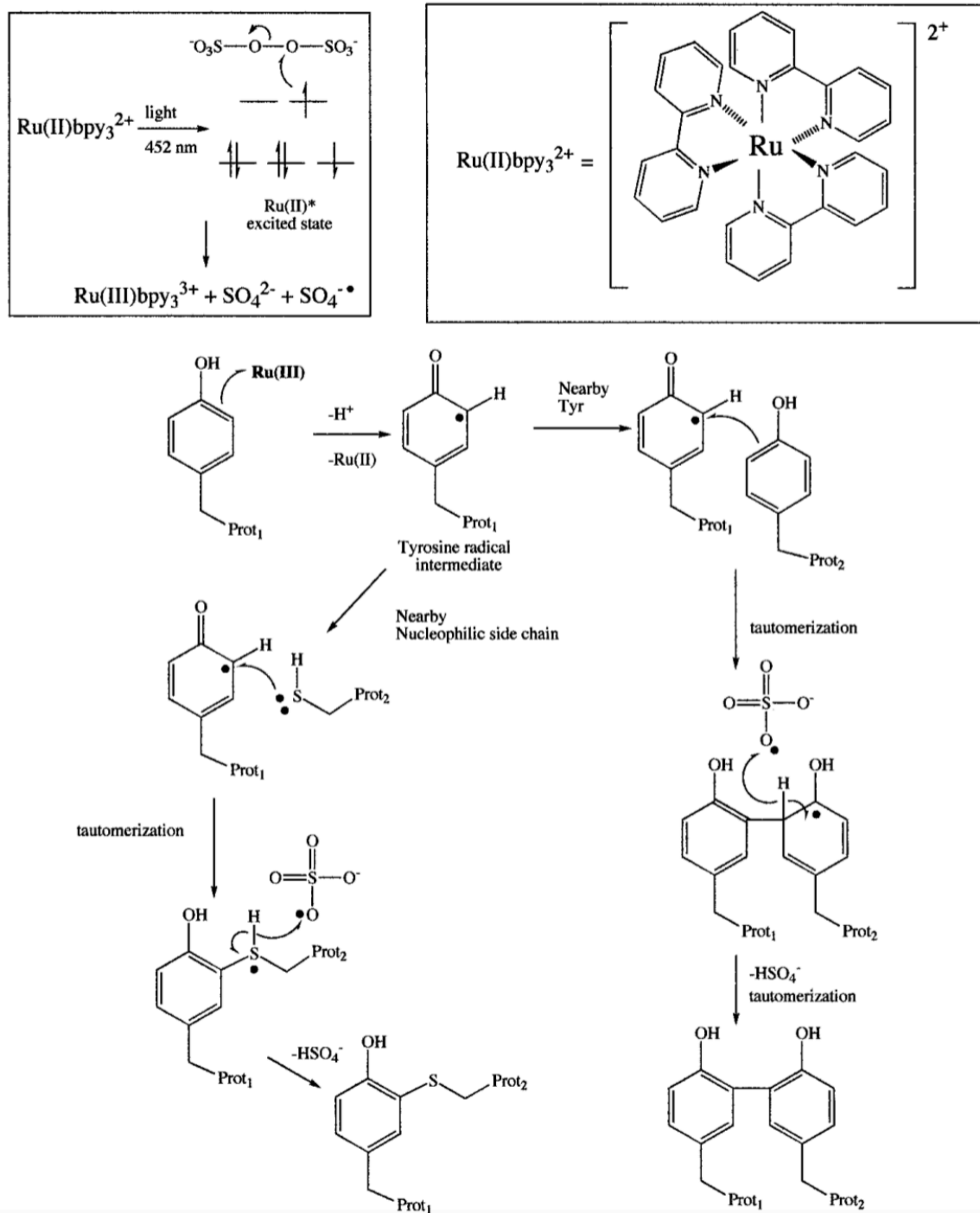


Figure 3.16 Mechanism of a photo-initiated tyrosine crosslinking reaction. [61]

Table 3.1 AT products synthesized using different feeding of L-tyr mole equivalents and their solubilization in aqueous media at RT.

| Sample | Tyr eq. | Absorbance | %Tyrosine | Solubility | | |
|--------|---------|--------------------------|-----------|------------|--------|--------|
| | | | | 3% w/v | 2% w/v | 1% w/v |
| AT1 | 0.5 | 0.7271 (± 0.1423) | 16.81 | x | ✓ | ✓ |
| AT2 | 1.0 | 0.7799 (± 0.1170) | 18.11 | x | ✓ | ✓ |
| AT3 | 1.5 | 0.9992 (± 0.1490) | 23.49 | x | x | ✓ |
| AT4 | 3.0 | 1.1309 (± 0.08062) | 26.73 | x | x | ✓ |

✓ homogeneous dispersion

x non-homogeneous dispersion

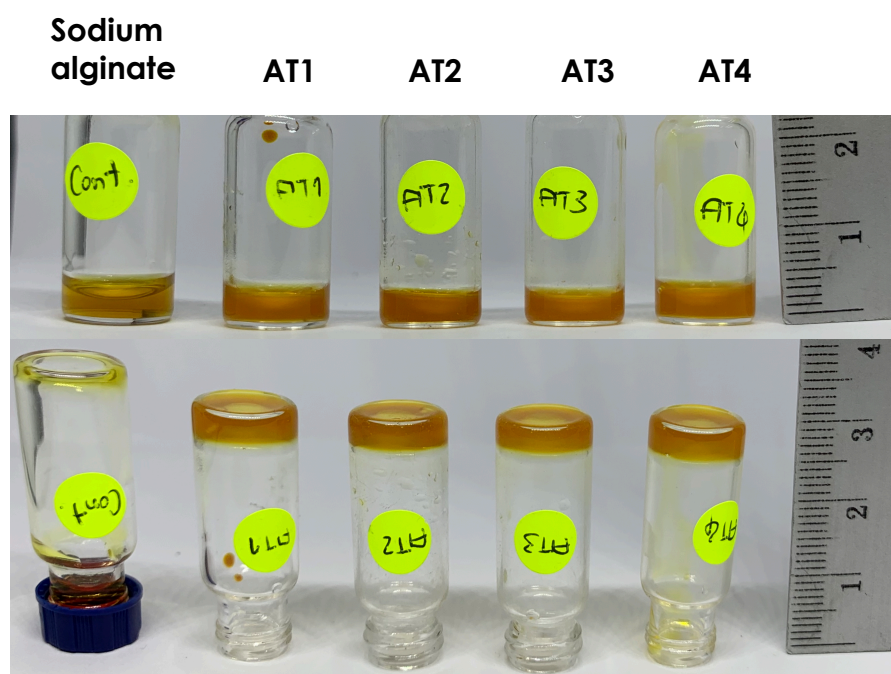


Figure 3.17 Gelation of products *via* visible light-induced crosslinking by using ruthenium as catalyst.

3.2.2 Synthesis of quaternized chitosan (QC)

To overcome the limitation of chitosan solubility in physiological condition, chitosan was modified by quaternization with GTMAC to introduce positively charged quaternary ammonium and improve solubility of the modified chitosan in aqueous media. FTIR spectra of chitosan and QC are illustrated in **Figure 3.1**. A signal of C-H bending appeared at 1475 cm^{-1}

suggesting that trimethyl entities were incorporated. Also, the band at 1581cm^{-1} of N-H bending that corresponds to the primary amino groups on chitosan shifted to approximately 1550cm^{-1} after the modification. In this way, the FTIR analysis confirmed the successful conjugation of GTMAC to chitosan.

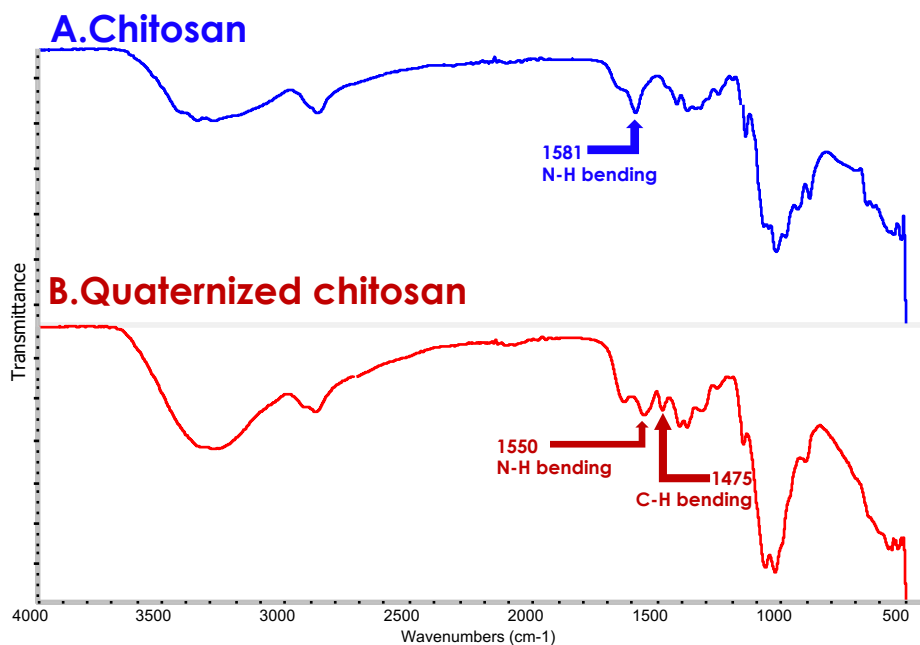


Figure 3.18 FT-IR spectra of A) chitosan and B) quaternized chitosan.

In addition, ^1H NMR analysis of chitosan and QC was performed in $\text{CF}_3\text{-COOH}$ and D_2O solution, respectively. The characteristic peaks of each functional group of chitosan and QC detected by ^1H -NMR are shown in **Figure 3.17**. The signal at 1.9 ppm was attributed to $-\text{COCH}_3$ from chitin and the peaks of $\text{H}_{3,4,5,6}$ in a range of 3.5-4.0 ppm were assigned to all protons in the pyranose ring of both chitosan and QC. However, peaks at 3.1 and 3.3 ppm were only found in QC spectrum, implying that $-\text{N}(\text{CH}_3)_3$ and $-\text{N-CH}_2-$ groups were incorporated, respectively. These evidently confirmed the successful synthesis of QC. Nevertheless, the glycidyltrimethylammonium content of QC needs to be evaluated and optimized for preparation of polysaccharide-based hydrogel in combination with OAT. For solubility test, QC can dissolve in PBS buffer pH 7.4 homogeneously at 2% w/v but chitosan cannot.

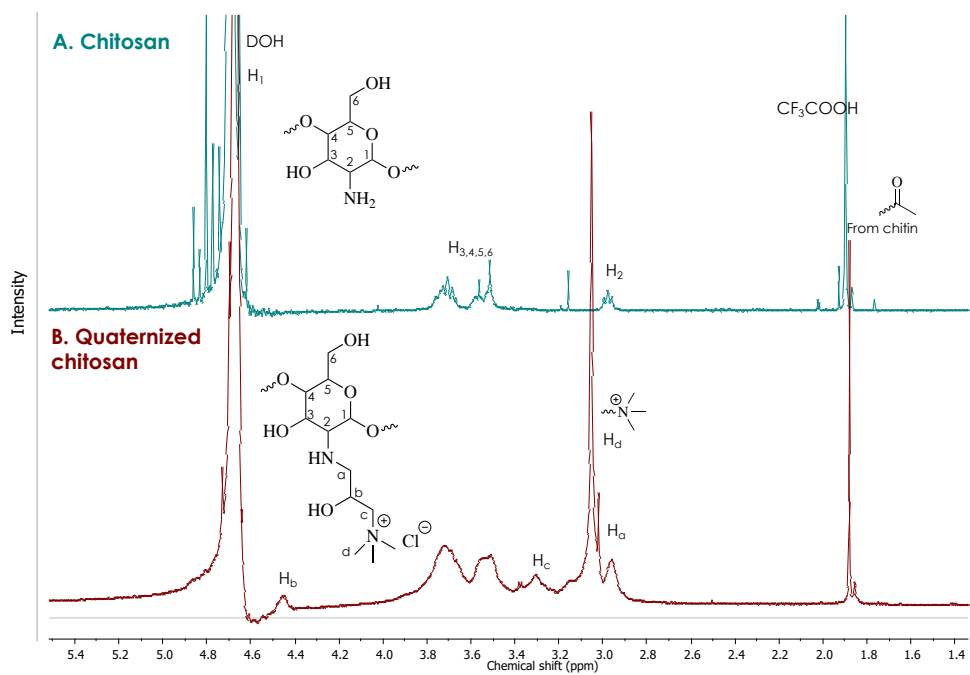


Figure 3.19 ¹H-NMR spectra of A) chitosan and B) quaternized chitosan in CF₃COOH and D₂O, respectively.

CHAPTER 4

CONCLUSIONS

In this project, we aimed to prepare polymeric hydrogels to be applied as bio-glue. For the polyphosphoester-based hydrogel, IPP monomer was successfully synthesized by reacting COP with IPA *via* nucleophilic substitution and was characterized by NMR spectroscopy. The P-TMP monomer can be synthesized but it cannot be effectively purified. ^{31}P -NMR analysis can identify species of phospholane of crude product and PA/PP ratio. PA species (*N*-attack) were more than PP (*O*-attack). Unfortunately, the purification methods such as flash column and silica gel plug cannot successfully purify the monomer. We suspect that P-TMP, which is cyclic phospholane, is sensitive to several nucleophiles such as water, silanol on column and also temperature to open the phospholane ring. In the future, we would like to find new ways to synthesize P-TMP monomer and perhaps use reverse-phase column as stationary phase for monomer purification.

For the polysaccharide-based hydrogel, we successfully synthesized tyrosine-modified alginate (AT) and hydrogelation *via* visible light-induced crosslinking by using ruthenium catalyst can be successfully achieved within 30 s. AT1 having %DS of 16.8% was chosen for further study because it can dissolve in water. To be able to form Schiff base linkage with QC, AT1 was oxidized by NaIO_4 into OAT. The presence of aldehyde groups of OAT was verified by the positive test against 2,4-DNP reagent. Chitosan was successfully modified by reacting with GTMAC and yield QC that can dissolve in pH 7.4 buffer with the highest concentration of 2%w/v. For the future work, we are going to identify an optimal gelation condition to form the soft hydrogel having double network *via* Schiff base linkage followed by visible light-induced crosslinking before mechanical tests.

REFERENCES

1. Singer, A. J.; Clark, R. A., Cutaneous wound healing. *The New England Journal of Medicine* **1999**, *341* (10), 738-746.
2. Nam, S.; Mooney, D., Polymeric Tissue Adhesives. *Chemical Reviews* **2021**.
3. Gurtner, G. C.; Werner, S.; Barrandon, Y.; Longaker, M. T., Wound repair and regeneration. *Nature* **2008**, *453* (7193), 314-321.
4. Annabi, N.; Tamayol, A.; Shin, S. R.; Ghaemmaghami, A. M.; Peppas, N. A.; Khademhosseini, A., Surgical Materials: Current Challenges and Nano-enabled Solutions. *Nano Today* **2014**, *9* (5), 574-589.
5. Ronald Januchowski, D. O.; W. Jordan Ferguson, O. M. S., III, The Clinical Use of Tissue Adhesives: A Review of the Literature. *Osteopathic Family Physician* **2014**, *6* (2).
6. von Fraunhofer, J. A.; Storey, R. S.; Stone, I. K.; Masterson, B. J., Tensile strength of suture materials. *Journal of Biomedical Materials Research* **1985**, *19* (5), 595-600.
7. Bouten, P. J. M.; Zonjee, M.; Bender, J.; Yauw, S. T. K.; van Goor, H.; van Hest, J. C. M.; Hoogenboom, R., The chemistry of tissue adhesive materials. *Progress in Polymer Science* **2014**, *39* (7), 1375-1405.
8. Duarte, A. P.; Coelho, J. F.; Bordado, J. C.; Cidade, M. T.; Gil, M. H., Surgical adhesives: Systematic review of the main types and development forecast. *Progress in Polymer Science* **2012**, *37* (8), 1031-1050.
9. Spotnitz, W. D.; Burks, S., Hemostats, sealants, and adhesives: components of the surgical toolbox. *Transfusion* **2008**, *48* (7), 1502-1516.
10. Spotnitz, W. D.; Burks, S., State-of-the-art review: Hemostats, sealants, and adhesives II: Update as well as how and when to use the components of the surgical toolbox. *Clinical and Applied Thrombosis/Hemostasis* **2010**, *16* (5), 497-514.
11. Spotnitz, W. D.; Burks, S., Hemostats, sealants, and adhesives III: a new update as well as cost and regulatory considerations for components of the surgical toolbox. *Transfusion* **2012**, *52* (10), 2243-2255.
12. Jarrett, P.; Coury, A., Tissue adhesives and sealants for surgical applications. *Joining and assembly of medical materials and devices* **2013**, 449-490.
13. Leggat, P. A.; Smith, D. R.; Kedjarune, U., Surgical applications of cyanoacrylate adhesives: a review of toxicity. *ANZ Journal of Surgery* **2007**, *77* (4), 209-213.

14. Kim, J. C.; Bassage, S. D.; Kempinski, M. H.; del Cerro, M.; Park, S. B.; Aquavella, J. V., Evaluation of tissue adhesives in closure of scleral tunnel incisions. *Journal of Cataract & Refractive Surgery* **1995**, *21* (3), 320-325.
15. Hino, M.; Ishiko, O.; Honda, K. I.; Yamane, T.; Ohta, K.; Takubo, T.; Tatsumi, N., Transmission of symptomatic parvovirus B19 infection by fibrin sealant used during surgery. *British Journal of Haematology* **2000**, *108* (1), 194-195.
16. Kawamura, M.; Sawafuji, M.; Watanabe, M.; Horinouchi, H.; Kobayashi, K., Frequency of transmission of human parvovirus B19 infection by fibrin sealant used during thoracic surgery. *Annals of Thoracic Surgery* **2002**, *73* (4), 1098-1100.
17. Steinbach, T.; Wurm, F. R., Poly(phosphoester)s: A New Platform for Degradable Polymers. *Angewandte Chemie International Edition in English* **2015**, *54* (21), 6098-6108.
18. Lapienis, G.; Penczek, S., Cationic Polymerization of 2-Alkoxy-2-oxo-1,3,2-dioxaphosphorinanes (1,3-Propylene Alkyl Phosphates). *Macromolecules* **1977**, *10* (6), 1301-1306.
19. Li, H.; He, J.; Zhang, M.; Liu, J.; Ni, P., Glucose-Sensitive Polyphosphoester Diblock Copolymer for an Insulin Delivery System. *ACS Biomaterials Science & Engineering* **2020**, *6* (3), 1553-1564.
20. Shin, M.; Ryu, J. H.; Park, J. P.; Kim, K.; Yang, J. W.; Lee, H., DNA/Tannic Acid Hybrid Gel Exhibiting Biodegradability, Extensibility, Tissue Adhesiveness, and Hemostatic Ability. *Advanced Functional Materials* **2015**, *25* (8), 1270-1278.
21. Iwasaki, Y.; Wachiralarpphathoon, C.; Akiyoshi, K., Novel Thermoresponsive Polymers Having Biodegradable Phosphoester Backbones. *Macromolecules* **2007**, *40* (23), 8136-8138.
22. Yu, F.; Cao, X.; Du, J.; Wang, G.; Chen, X., Multifunctional Hydrogel with Good Structure Integrity, Self-Healing, and Tissue-Adhesive Property Formed by Combining Diels–Alder Click Reaction and Acylhydrazone Bond. *ACS Applied Materials & Interfaces* **2015**, *7* (43), 24023-24031.
23. Liu, Y.; Wong, C.-W.; Chang, S.-W.; Hsu, S.-h., An injectable, self-healing phenol-functionalized chitosan hydrogel with fast gelling property and visible light-crosslinking capability for 3D printing. *Acta Biomaterialia* **2021**, *122*, 211-219.
24. Yang, X.; Liu, G.; Peng, L.; Guo, J.; Tao, L.; Yuan, J.; Chang, C.; Wei, Y.; Zhang, L., Highly Efficient Self-Healable and Dual Responsive Cellulose-Based

- Hydrogels for Controlled Release and 3D Cell Culture. *Advanced Functional Materials* **2017**, *27* (40), 1703174.
25. Li, N.; Yang, X.; Liu, W.; Xi, G.; Wang, M.; Liang, B.; Ma, Z.; Feng, Y.; Chen, H.; Shi, C., Tannic Acid Cross-linked Polysaccharide-Based Multifunctional Hemostatic Microparticles for the Regulation of Rapid Wound Healing. *Macromolecular Bioscience* **2018**, *18* (11), e1800209.
 26. Zhao, X.; Wu, H.; Guo, B.; Dong, R.; Qiu, Y.; Ma, P. X., Antibacterial anti-oxidant electroactive injectable hydrogel as self-healing wound dressing with hemostasis and adhesiveness for cutaneous wound healing. *Biomaterials* **2017**, *122*, 34-47.
 27. Chirkov, S. N., The Antiviral Activity of Chitosan (Review). *Applied Biochemistry and Microbiology* **2002**, *38* (1), 1-8.
 28. Zhang, J.; Xia, W.; Liu, P.; Cheng, Q.; Tahirou, T.; Gu, W.; Li, B., Chitosan modification and pharmaceutical/biomedical applications. *Marine Drugs* **2010**, *8* (7), 1962-1987.
 29. Liu, P.; Meng, W.; Wang, S.; Sun, Y.; Ashraf, M. A., Quaternary ammonium salt of chitosan: preparation and antimicrobial property for paper. *Open Medicine* **2015**, *10* (1), 473-478.
 30. Kumirska, J.; Weinhold, M. X.; Thöming, J.; Stepnowski, P., Biomedical Activity of Chitin/Chitosan Based Materials—Influence of Physicochemical Properties Apart from Molecular Weight and Degree of N-Acetylation. *Polymers* **2011**, *3* (4).
 31. Sun, J.; Tan, H., Alginate-Based Biomaterials for Regenerative Medicine Applications. *Materials (Basel)* **2013**, *6* (4), 1285-1309.
 32. Stevens, M. M.; Qanadilo, H. F.; Langer, R.; Prasad Shastri, V., A rapid-curing alginate gel system: utility in periosteum-derived cartilage tissue engineering. *Biomaterials* **2004**, *25* (5), 887-894.
 33. Augst, A. D.; Kong, H. J.; Mooney, D. J., Alginate hydrogels as biomaterials. *Macromolecular Bioscience* **2006**, *6* (8), 623-633.
 34. Bouhadir, K. H.; Lee, K. Y.; Alsberg, E.; Damm, K. L.; Anderson, K. W.; Mooney, D. J., Degradation of partially oxidized alginate and its potential application for tissue engineering. *Biotechnology Progress* **2001**, *17* (5), 945-950.
 35. Yuan, L.; Wu, Y.; Fang, J.; Wei, X.; Gu, Q.; El-Hamshary, H.; Al-Deyab, S. S.; Morsi, Y.; Mo, X., Modified alginate and gelatin cross-linked hydrogels for soft tissue adhesive. *Artificial Cells, Nanomedicine, and Biotechnology* **2017**, *45* (1), 76-83.

36. Taboada, G. M.; Yang, K.; Pereira, M. J. N.; Liu, S. S.; Hu, Y.; Karp, J. M.; Artzi, N.; Lee, Y., Overcoming the translational barriers of tissue adhesives. *Nature Reviews Materials* **2020**, *5* (4), 310-329.
37. Awaja, F.; Gilbert, M.; Kelly, G.; Fox, B.; Pigram, P. J., Adhesion of polymers. *Progress in Polymer Science* **2009**, *34* (9), 948-968.
38. Yang, J.; Cohen Stuart, M. A.; Kamperman, M., Jack of all trades: versatile catechol crosslinking mechanisms. *Chemical Society Reviews* **2014**, *43* (24), 8271-8298.
39. Lee, H. A.; Park, E.; Lee, H., Polydopamine and Its Derivative Surface Chemistry in Material Science: A Focused Review for Studies at KAIST. *Advanced Materials* **2020**, *32* (35), 1907505.
40. Anselmo, A. C.; Modery-Pawłowski, C. L.; Menegatti, S.; Kumar, S.; Vogus, D. R.; Tian, L. L.; Chen, M.; Squires, T. M.; Sen Gupta, A.; Mitragotri, S., Platelet-like nanoparticles: mimicking shape, flexibility, and surface biology of platelets to target vascular injuries. *ACS Nano* **2014**, *8* (11), 11243-11253.
41. Yang, X.; Liu, W.; Li, N.; Wang, M.; Liang, B.; Ullah, I.; Luis Neve, A.; Feng, Y.; Chen, H.; Shi, C., Design and development of polysaccharide hemostatic materials and their hemostatic mechanism. *Biomaterials Science* **2017**, *5* (12), 2357-2368.
42. Pallister, M. W., Haematology. *Scion Publishing* **2010**, 336–347.
43. Behrens, A. M.; Sikorski, M. J.; Kofinas, P., Hemostatic strategies for traumatic and surgical bleeding. *Journal of Biomedical Materials Research Part A* **2014**, *102* (11), 4182-4194.
44. Yang, J.; Lv, J.; Gao, B.; Zhang, L.; Yang, D.; Shi, C.; Guo, J.; Li, W.; Feng, Y., Modification of polycarbonateurethane surface with poly (ethylene glycol) monoacrylate and phosphorylcholine glyceraldehyde for anti-platelet adhesion. *Frontiers of Chemical Science and Engineering* **2014**, *8* (2), 188-196.
45. Hajosch, R.; Suckfuell, M.; Oesser, S.; Ahlers, M.; Flechsenhar, K.; Schlosshauer, B., A novel gelatin sponge for accelerated hemostasis. *Journal of Biomedical Materials Research Part B: Applied Biomaterials* **2010**, *94* (2), 372-379.
46. Nagy, A.; Harrison, A.; Sabbani, S.; Munson, R. S., Jr.; Dutta, P. K.; Waldman, W. J., Silver nanoparticles embedded in zeolite membranes: release of silver ions and mechanism of antibacterial action. *International Journal of Nanomedicine* **2011**, *6*, 1833-1852.

47. Yilmaz Atay, H., Antibacterial Activity of Chitosan-Based Systems. *Functional Chitosan* **2020**, 457-489.
48. Hosseinnejad, M.; Jafari, S. M., Evaluation of different factors affecting antimicrobial properties of chitosan. *International Journal of Biological Macromolecules* **2016**, *85*, 467-475.
49. Wang, Z.; An, G.; Zhu, Y.; Liu, X.; Chen, Y.; Wu, H.; Wang, Y.; Shi, X.; Mao, C., 3D-printable self-healing and mechanically reinforced hydrogels with host-guest non-covalent interactions integrated into covalently linked networks. *Materials Horizons* **2019**, *6* (4), 733-742.
50. Sakai, S.; Ohi, H.; Hotta, T.; Kamei, H.; Taya, M., Differentiation potential of human adipose stem cells bioprinted with hyaluronic acid/gelatin-based bioink through microextrusion and visible light-initiated crosslinking. *Biopolymers* **2018**, *109* (2).
51. Bourke, S. L.; Al-Khalili, M.; Briggs, T.; Michniak, B. B.; Kohn, J.; Poole-Warren, L. A., A photo-crosslinked poly(vinyl alcohol) hydrogel growth factor release vehicle for wound healing applications. *AAPS PharmSciTech* **2003**, *5* (4), E33.
52. Elvin, C. M.; Vuocolo, T.; Brownlee, A. G.; Sando, L.; Huson, M. G.; Liyou, N. E.; Stockwell, P. R.; Lyons, R. E.; Kim, M.; Edwards, G. A.; Johnson, G.; McFarland, G. A.; Ramshaw, J. A. M.; Werkmeister, J. A., A highly elastic tissue sealant based on photopolymerised gelatin. *Biomaterials* **2010**, *31* (32), 8323-8331.
53. Hiranphinyophat, S.; Asaumi, Y.; Fujii, S.; Iwasaki, Y., Surface Grafting Polyphosphoesters on Cellulose Nanocrystals To Improve the Emulsification Efficacy. *Langmuir* **2019**, *35* (35), 11443-11451.
54. Porto, R. S.; Vasconcellos, M. L. A. A.; Ventura, E.; Coelho, F., Diastereoselective of Allylic Diols Derived from Baylis-Hillman Adducts. *Synthesis* **2005**, *2005* (14), 2297-2306.
55. Zhang, S.; Wang, H.; Shen, Y.; Zhang, F.; Seetho, K.; Zou, J.; Taylor, J. S.; Dove, A. P.; Wooley, K. L., A Simple and Efficient Synthesis of an Acid-labile Polyphosphoramidate by Organobase-catalyzed Ring-Opening Polymerization and Transformation to Polyphosphoester Ionomers by Acid Treatment. *Macromolecules* **2013**, *46* (13), 5141-5149.
56. Banks, S. R.; Enck, K.; Wright, M.; Opara, E. C.; Welker, M. E., Chemical Modification of Alginate for Controlled Oral Drug Delivery. *Journal of Agricultural and Food Chemistry* **2019**, *67* (37), 10481-10488.

57. Cho, J.; Grant, J.; Piquette-Miller, M.; Allen, C., Synthesis and Physicochemical and Dynamic Mechanical Properties of a Water-Soluble Chitosan Derivative as a Biomaterial. *Biomacromolecules* **2006**, *7* (10), 2845-2855.
58. Seong, H.-S.; Whang, H. S.; Ko, S.-W., Synthesis of a quaternary ammonium derivative of chito-oligosaccharide as antimicrobial agent for cellulosic fibers. *Journal of Applied Polymer Science* **2000**, *76* (14), 2009-2015.
59. Wang, H.; Su, L.; Li, R.; Zhang, S.; Fan, J.; Zhang, F.; Nguyen, T. P.; Wooley, K. L., Polyphosphoramidates That Undergo Acid-Triggered Backbone Degradation. *ACS Macro Letters* **2017**, *6* (3), 219-223.
60. Iwasaki, Y.; Bunuasunthon, S.; Hoven, V. P., Protein patterning with antifouling polymer gel platforms generated using visible light irradiation. *Chemical Communications* **2020**, *56* (41), 5472-5475.
61. Fancy, D. A.; Kodadek, T., Chemistry for the analysis of protein–protein interactions: Rapid and efficient cross-linking triggered by long wavelength light. *Proceedings of the National Academy of Sciences* **1999**, *96* (11), 6020.
62. Bauer, K. N.; Tee, H. T.; Velencoso, M. M.; Wurm, F. R., Main-chain (phosphoester)s: History, syntheses, degradation, bio-and flame-retardant applications. *Progress in Polymer Science* **2017**, *73*, 61-122.

VITA

Mr. Thanapon Puangniyom was born on September 14, 1998 in Samut Sakhon, Thailand. He graduated from Suksanareewittaya school in Mathematics – Science program, Bangkok in 2016. Currently, He started as a bachelor's degree student with a major in Chemistry, Faculty of Science, Chulalongkorn University in the academic year of 2017. He received a scholarship from Development and Promotion of Science and Technology Talents (DPST) scholarship in the academic year of 2018. He will graduate in June 2021 for his bachelor's degree. His current address is 99/350 Rama 2 road, Bang Nam Chuet, Mueang Samut Sakhon, Samut Sakhon, Thailand, 74000. E-mail: tinglythanapon@gmail.com